# Quasiparticle-Vibration Couplings in Rotating Triaxial Odd-$A$ Nuclei

Masayuki MATSUZAKI, Yoshifumi R. SHIMIZU*
and Kenichi MATSUYANAGI

*Department of Physics, Kyoto University, Kyoto 606*
*\*Department of Physics, Kyushu University, Fukuoka 812*

A new microscopic model which takes into account both the static and dynamic triaxial deformations in the high-spin states of odd-$A$ nuclei is developed. The model is based on the rotating shell model and treats the quasiparticle-vibration couplings in the uniformly rotating frame of reference. Effects of the static and dynamic triaxial deformations on the signature splitting of the quasiparticle energies and on the signature dependence of $B(M1)$, $B(E2; I \rightarrow I-1)$ and $B(E2; I \rightarrow I-2)$ for the transitions within the unique-parity bands in odd-$A$ nuclei are discussed. Numerical examples are presented for odd-$Z$ nuclei $^{157}$Ho, $^{159}$Tm and $^{161,165}$Lu, and for odd-$N$ nuclei $^{161}$Dy, $^{167}$Er and $^{161,163,167}$Yb to which experimental data for $B(M1)$ and $B(E2)$ are available.

## § 1. Introduction

The main purpose of this paper is to extend the traditional quasiparticle-vibration coupling model for non-rotating nuclei[1],[2] into the case of rapidly rotating nuclei by formulating it in the reference frame which is uniformly rotating with rotational frequency $\omega_{rot}$. It is intended to use this model for analyzing the dynamical interplay in odd-$A$ nuclei between aligned quasiparticle excitations and vibrational excitations in the near-yrast region with large angular momentum. In this paper, among the various vibrational modes, we focus our attention on the "gamma" vibrations which represent dynamical shape fluctuations in the gamma degree of freedom. Since we treat odd-$A$ nuclei whose equilibrium shapes are (in general) triaxial and which are rotating, the "gamma" vibrational modes do not have definite $K$ quantum number and may contain the components corresponding to the wobbling modes[3] characteristic to nuclei having static triaxial shapes. We, therefore, call these vibrations "generalized-gamma vibrations" in order to distinguish them from the familiar gamma vibrations with $K = \pm 2$ which represent the shape fluctuations away from the axially symmetric equilibrium shape.

The motive for developing this model lies in the recent experimental progress[4]~[13] in measuring both the stretched and non-stretched $E2$ transition probabilities as well as the $M1$ transitions between very high-spin states in odd-$A$ nuclei in the rare-earth region. As was pointed out by Hamamoto and Mottelson,[14],[15] these experimental data contain information useful to identify the static and dynamic triaxial deformations and their relations to rapid rotations.

Our model is based on the rotating shell model (RSM)[16],[17] which is an extension of the familiar cranked shell model[18],[19] in that the variation of the pairing gap $\Delta$ and the deformation parameters $(\beta, \gamma)$ as functions of $\omega_{rot}$ is taken into account for each

rotational band.   One of the merits of our microscopic approach is that it can be easily applied to high-spin states involving many aligned quasiparticles.   On the other hand, its main limitation is that the generalized-gamma vibrations are treated within the small-amplitude approximation of the RPA.   Thus, our microscopic model may be best suited to the description of rotational bands in the near-yrast region of odd-$A$ nuclei which have rather stable minimum somewhere in the $(\beta, \gamma)$ plane.

The formulation of our model consists of the following four steps:

1)   Our first task is to construct a diabatic quasiparticle representation for a deformed single-particle potential which is uniformly rotating about the $x$-axis with rotational frequency $\omega_{\text{rot}}$.   The diabatic basis for the RSM enables us to unambiguously specify individual rotational bands in which internal structures of the quasiparticle state vectors smoothly change as functions of $\omega_{\text{rot}}$.[19]

2)   The residual interactions between quasiparticles are treated by means of the RPA in the rotating frame.   This step determines the normal modes of vibration in even-even nuclei.

3)   Then we treat the couplings in odd-$A$ nuclei between the aligned quasiparticles and the generalized-gamma vibrations (obtained above) in the same manner as in the traditional quasiparticle-vibration coupling models.[1],[2]

4)   The most crucial point of our approach is the treatment of the "Nambu-Goldstone modes", $\Gamma^{\dagger}$ and $\Gamma$, in the RPA, which reorient the angular momentum of the collective rotation.   We extend Marshalek's prescription[20] into odd-$A$ nuclei and replace these modes with the exact angular-momentum operators.   This replacement corresponds to the fact that the state vectors in the laboratory frame are constructed in a direct product form of the rotational and the internal wave function in just the same manner as in the well-known particle-rotor model.[3]   Thus, our model may also be regarded as a particular version of the particle-rotor model, in which the basis of the internal state vectors is determined by the RSM as a function of $\omega_{\text{rot}}$.

Details of the formulation in each step mentioned above are given in § 2.   In this section, we also give microscopic expressions for the intrinsic $E2$ and $M1$ operators. These formulae may be useful to the analysis of 1) the effects of static and dynamic triaxial deformations on the $B(E2)$ values with $\Delta I = 1$ which connect the favoured bands to the unfavoured bands (and v.v.), and 2) the effects of aligned quasiparticles on $B(M1)$ values.   Details of the computational procedure are described in § 3. Some typical results of numerical calculation are presented in § 4 for 1) nuclei with the $h_{11/2}$ odd protons and 2) nuclei with the $i_{13/2}$ odd neutrons.   Concluding remarks are given in § 5.


## § 2.   Formulation of model

### 2.1.   *Diabatic quasiparticle basis for use in the rotating shell model*

We start from a single-particle potential $\bar{h}_{\text{sp}}$ which is deformed with respect to both the pairing and the quadrupole degrees of freedom:

$$\bar{h}_{\text{sp}} = \bar{h}_{\text{def}} - \Delta(\hat{P}^{\dagger} + \hat{P}) - \lambda\hat{N}, \qquad (2\cdot1)$$

where $\hat{h}_{\mathrm{def}}$ is the modified-harmonic-oscillator potential defined by

$$\hat{h}_{\mathrm{def}} = \hat{h}_{\mathrm{sph}}(\boldsymbol{x} \to \tilde{\boldsymbol{x}}, \boldsymbol{p}) , \tag{2.2}$$

$$\hat{h}_{\mathrm{sph}} = \sum_{n=1}^{A} \left\{ \frac{\boldsymbol{p}^2}{2M} + \frac{1}{2} M\omega_0^2 \boldsymbol{x}^2 + v_{ls}\boldsymbol{l}\cdot\boldsymbol{s} + v_{ll}(\boldsymbol{l}^2 - \langle \boldsymbol{l}^2 \rangle_N) \right\}_n . \tag{2.3}$$

Here, $\hat{P}$ and $\hat{N}$ are the conventional nucleon-pair and nucleon-number operators, respectively. They are treated separately for protons and neutrons. In Eq. (2·2) the notation $\boldsymbol{x} \to \tilde{\boldsymbol{x}}$ means that the coordinates $x_i(i=1,2,3)$ are replaced by the doubly stretched coordinates $\tilde{x}_i \equiv (\omega_i/\omega_0)x_i$. We consider triaxial quadrupole deformations so that the frequencies $\omega_i$ with $i=1,2$ and $3$ of the modified-harmonic-oscillator are not equal in general.

Let us consider a situation where the nucleus is uniformly rotating with rotational frequency $\omega_{\mathrm{rot}}$ about the $x$-axis (the 1st axis) defined with respect to the single-particle potential $\hat{h}_{\mathrm{sp}}$. To describe such a uniformly rotating nucleus, we consider a time-dependent state vector which has a form familiar in the Hartree-Bogoliubov theory:

$$|\phi(I,\theta)\rangle = e^{-i\theta \hat{J}_x} e^{i\hat{G}} |\phi_0\rangle , \tag{2.4}$$

where $|\phi_0\rangle$ is the BCS ground state for $\hat{h}_{\mathrm{sp}}$ and $\theta = \omega_{\mathrm{rot}}t$. We expand the unknown one-body operator $\hat{G}$ in a power series of $\omega_{\mathrm{rot}}$, i.e.,

$$\hat{G} = \hat{G}^{(0)} + \omega_{\mathrm{rot}}\hat{G}^{(1)} + \omega_{\mathrm{rot}}^2 \hat{G}^{(2)} + \cdots , \tag{2.5}$$

and successively determine $\hat{G}^{(n)}$ so as to satisfy the following basic equations:

(i)  $I = -\dfrac{\partial \mathcal{H}'}{\partial \omega_{\mathrm{rot}}}$

   with  $\mathcal{H}' = \langle \phi_0 | e^{-i\hat{G}}(\hat{h}_{\mathrm{sp}} - \omega_{\mathrm{rot}}\hat{J}_x)e^{i\hat{G}} | \phi_0 \rangle ,$ \tag{2.6}

(ii)  $\delta \langle \phi_0 | e^{-i\hat{G}}(\hat{h}_{\mathrm{sp}} - \omega_{\mathrm{rot}}\hat{J}_x)e^{i\hat{G}} | \phi_0 \rangle = 0 ,$ \tag{2.7}

(iii)  $\langle \phi_0 | e^{-i\hat{G}}\hat{J}_x e^{i\hat{G}} | \phi_0 \rangle = I ,$

$$\left.\langle \phi_0 | e^{-i\hat{G}}\frac{\partial}{\partial \omega_{\mathrm{rot}}}e^{i\hat{G}} | \phi_0 \rangle = 0 . \right\} \tag{2.8}$$

The above basic equations are derived by applying the selfconsistent-collective-coordinate method[21] to the particular problem under consideration. A method of solving this set of equations is described in detail in Ref. 22) (see also Ref. 23)). It is found[23] that a cutoff of the $\omega_{\mathrm{rot}}$-expansion in Eq. (2·5) results in a diabatic level diagram (in place of the adiabatic one) for the quasiparticle energies in the rotating frame. As is well known, the diabatic basis enables us to unambiguously specify individual rotational bands whose internal wave functions smoothly change as functions of $\omega_{\mathrm{rot}}$.[19] In this way, we obtain a single-particle Hamiltonian $\hat{h}'_{\mathrm{sp}}$ describing independent quasiparticle motions in the deformed potential $\hat{h}_{\mathrm{sp}}$ which is now rotating with the rotational frequency $\omega_{\mathrm{rot}}$:

$$\hat{h}'_{\mathrm{sp}} = \mathrm{const} + \sum_{\mu} E_{\mu} a_{\mu}^{\dagger} a_{\mu} + \sum_{\bar{\mu}} E_{\bar{\mu}} a_{\bar{\mu}}^{\dagger} a_{\bar{\mu}} , \tag{2.9}$$

where $(a_\mu^\dagger, a_\mu)$ and $(a_{\bar\mu}^\dagger, a_{\bar\mu})$ are the diabatic quasiparticle creation and annihilation operators with signature $\alpha = 1/2$ ($r \equiv e^{-i\pi\alpha} = -i$) and $\alpha = -1/2$ ($r = +i$), respectively. They are determined, together with their energies $E_\mu$ and $E_{\bar\mu}$, as smooth functions of $\omega_{\text{rot}}$.[*]

To describe individual rotational bands, we have to carefully identify the quasiparticle configurations across the band-crossing region such that their internal structures smoothly change as functions of $\omega_{\text{rot}}$. This is done in the following way. Let us denote the quasiparticles defined with respect to the yrast configuration $|\phi_y\rangle$ by $(\overset{\circ}{a}_\mu^\dagger, \overset{\circ}{a}_{\bar\nu}^\dagger)$; i.e.,

$$\overset{\circ}{a}_\mu|\phi_y\rangle = \overset{\circ}{a}_{\bar\nu}|\phi_y\rangle = 0 , \tag{2.10}$$

where $|\phi_y\rangle$ is constructed to be the lowest-energy configuration at a given value of $\omega_{\text{rot}}$. Then, the quasiparticle configurations describing individual rotational bands take in general the following form:

$$|\phi_{\text{band}}\rangle = (\prod_{\mu=1}^{n_+} \overset{\circ}{a}_\mu^\dagger)(\prod_{\bar\nu=1}^{n_-} \overset{\circ}{a}_{\bar\nu}^\dagger)|\phi_y\rangle \quad \text{for } \omega_{\text{cri}}^{(i)} < \omega_{\text{rot}} < \omega_{\text{cri}}^{(j)} . \tag{2.11}$$

Note that the explicit form of $|\phi_{\text{band}}\rangle$ changes whenever the rotational band under consideration crosses with another band; for instance, the configuration corresponding to the $g$-band changes as

$$|\phi_g\rangle = \begin{cases} |\phi_y\rangle , & 0 \leq \omega_{\text{rot}} \leq \omega_{\text{cri}}^{(1)} , \\ \overset{\circ}{a}_A^\dagger \overset{\circ}{a}_B^\dagger|\phi_y\rangle , & \omega_{\text{cri}}^{(1)} \leq \omega_{\text{rot}} \leq \omega_{\text{cri}}^{(2)} , \\ \overset{\circ}{a}_A^\dagger \overset{\circ}{a}_D^\dagger|\phi_y\rangle , & \omega_{\text{cri}}^{(2)} \leq \omega_{\text{rot}} \leq \omega_{\text{cri}}^{(3)} , \\ \cdots & \end{cases} \tag{2.12}$$

On the other hand, the configuration for the $s$-band changes as

$$|\phi_s\rangle = \begin{cases} \overset{\circ}{a}_A^\dagger \overset{\circ}{a}_B^\dagger|\phi_y\rangle , & 0 \leq \omega_{\text{rot}} \leq \omega_{\text{cri}}^{(1)} , \\ |\phi_y\rangle , & \omega_{\text{cri}}^{(1)} \leq \omega_{\text{rot}} \leq \omega_{\text{cri}}^{(4)} , \\ \cdots & \end{cases} \tag{2.13}$$

Here the suffices $A, B, \cdots$ are the familiar notations[24] labelling the quasiparticle states with unique-parity.

The equilibrium deformations are determined as functions of $\omega_{\text{rot}}$ for each rotational band in even-even nuclei to simultaneously satisfy the following self-consistency conditions:

$$G\langle\phi_{\text{band}}|\hat{P}|\phi_{\text{band}}\rangle = \Delta , \qquad \langle\phi_{\text{band}}|\hat{N}|\phi_{\text{band}}\rangle = N$$

$$\text{for both protons and neutrons} , \tag{2.14}$$

$$(\omega_1^{\text{eff}})^2\langle\phi_{\text{band}}|\sum_{n=1}^A (x_1)_n^2|\phi_{\text{band}}\rangle = (\omega_2^{\text{eff}})^2\langle\phi_{\text{band}}|\sum_{n=1}^A (x_2)_n^2|\phi_{\text{band}}\rangle$$

$$= (\omega_3^{\text{eff}})^2\langle\phi_{\text{band}}|\sum_{n=1}^A (x_3)_n^2|\phi_{\text{band}}\rangle , \tag{2.15}$$

---

[*] Their precise definitions are given by Eq. (2.19) below.

under the volume-conservation condition $\omega_1^{\text{eff}} \omega_2^{\text{eff}} \omega_3^{\text{eff}} = \omega_0^3$, where $\omega_i^{\text{eff}} = \sqrt{\omega_i^2 - \omega_{\text{rot}}^2}$ for $i=2$ and 3, and $\omega_1^{\text{eff}} = \omega_1$. Equation (2·15) results from the semiclassical require- ment that the velocity distribution in the rotating frame be isotropic in average.[25] This equation determines the frequency $\omega_i$ of the potential, from which the ordinary deformation parameters $(\beta, \gamma)$ are immediately obtained.[25]

In this way, we obtain the diabatic quasiparticle representation whose equili- brium deformations are selfconsistently determined as functions of $\omega_{\text{rot}}$.

## 2.2.  The RPA in the uniformly rotating frame

The residual interactions that are consistent, in the sense of the Landau-Migdal theory, with the single-particle Hamiltonian (2·9) are given by

$$\hat{H}_{\text{int}} = \hat{H}_{\text{P}} + \hat{H}_{\text{QQ}}, \tag{2·16}$$

$$\hat{H}_{\text{P}} = -G\tilde{P}^\dagger \tilde{P} \quad \text{for both protons and neutrons}, \tag{2·17}$$

$$\hat{H}_{\text{QQ}} = -\frac{1}{2} \sum_{K=0,1,2} \kappa_K^{(+)} \tilde{Q}_K^{(+)\dagger} \tilde{Q}_K^{(+)} - \frac{1}{2} \sum_{K=1,2} \kappa_K^{(-)} \tilde{Q}_K^{(-)\dagger} \tilde{Q}_K^{(-)}, \tag{2·18}$$

where $\tilde{P} \equiv \hat{P} - \langle \phi_{\text{band}} | \hat{P} | \phi_{\text{band}} \rangle$ and $\tilde{Q}_K^{(\pm)}$ are the quadrupole operators that are defined in terms of the doubly stretched coordinates $x_i''$ associated with the rotating deformed potential, i.e., $x_i'' \equiv (\omega_i^{\text{eff}}/\omega_0) x_i$. At the equilibrium deformation where Eq. (2·15) holds, we have the properties $\langle \tilde{Q}_K^{(\pm)} \rangle = 0$ for all $K$.

To describe vibrational excitations built on a given rotational band $|\phi_{\text{band}}\rangle$ in even-even nuclei, it is convenient to use the quasiparticle operators $(a_\mu^\dagger, a_\nu^\dagger)$ defined with respect to this band:

$$a_\mu |\phi_{\text{band}}\rangle = 0 ; \quad \mu = 1, 2, \cdots, \Omega - n_{\text{B}},$$

$$a_{\bar{\nu}} |\phi_{\text{band}}\rangle = 0 ; \quad \bar{\nu} = 1, 2, \cdots, \Omega + n_{\text{B}}, \tag{2·19}$$

where $n_{\text{B}}$ is the blocking number of this band. These new quasiparticle operators are obtained from those defined by Eq. (2·10) through the following procedure.[16],[17] Let $2\Omega$ be the total number of single-particle states. Then, as is well known, the Hartree-Bogoliubov equation has $4\Omega$ solutions. If we identify $\Omega$ positive-energy solutions as physical solutions for both signature sectors ($\alpha = 1/2$ and $-1/2$), the quasiparticle vacuum coincides with the yrast configuration. Let $(n_\mu, n_{\bar{\nu}})$ be the occupation numbers of the quasiparticles ($\overset{\circ}{a}{}_\mu^\dagger, \overset{\circ}{a}{}_{\bar{\nu}}^\dagger$) in the configuration $|\phi_{\text{band}}\rangle$. Then the quasiparticle operators defined by (2·19) are obtained from the original quasiparti- cles by the following replacements:

$$\left. \begin{array}{l} (-E_\mu, V_\mu, U_\mu) \longrightarrow (E_{\overline{\Omega+\mu}}, \bar{U}_{\Omega+\mu}, \bar{V}_{\Omega+\mu}), \\ (-E_{\bar{\nu}}, \bar{V}_\nu, \bar{U}_\nu) \longrightarrow (E_{\Omega+\nu}, U_{\Omega+\nu}, V_{\Omega+\nu}) \end{array} \right\} \tag{2·20}$$

for the states with $n_\mu = 1$ and $n_{\bar{\nu}} = 1$, respectively. The other states with $n_\mu = n_{\bar{\nu}} = 0$ remain the same. Thus, the annihilation operators $\overset{\circ}{a}{}_\mu(\overset{\circ}{a}{}_{\bar{\nu}})$ for the states with $n_\mu = 1$ ($n_{\bar{\nu}} = 1$) are now replaced by the creation operators $a_{\overline{\Omega+\mu}}^\dagger (a_{\Omega+\nu}^\dagger)$ with negative energies and with opposite signature.

The RPA excitation operators $X_n^{(\pm)\dagger}$ are constructed in terms of the new quasiparticle operators as

$$X_n^{(\pm)\dagger} = \sum_{(\alpha\beta)} \{\psi_n^{(\pm)}(\alpha\beta) a_\alpha^\dagger a_\beta^\dagger + \varphi_n^{(\pm)}(\alpha\beta) a_\beta a_\alpha\}, \tag{2.21}$$

where $(\alpha\beta)=(\mu\bar{\nu})$ for the $\alpha=0$ $(r=+1)$ sector, and $(\alpha\beta)=(\mu\nu)$ or $(\bar{\mu}\bar{\nu})$ for the $\alpha=1$ $(r=-1)$ sector. The excitation energies $\hbar\omega_n^{(\pm)}$ and the amplitudes, $\psi_n^{(\pm)}(\alpha\beta)$ and $\varphi_n^{(\pm)}(\alpha\beta)$, are determined by solving the RPA equation of motion $[\hat{h}'_{\rm sp}+\hat{H}_{\rm int}, X_n^{(\pm)\dagger}]_{\rm RPA} = \hbar\omega_n^{(\pm)} X_n^{(\pm)\dagger}$ and by the normalization condition $\langle\phi_{\rm band}|[X_n^{(\pm)}, X_{n'}^{(\pm)\dagger}]|\phi_{\rm band}\rangle=\delta_{nn'}$. In this way, we obtain normal modes of vibration built on a given rotational band $|\phi_{\rm band}\rangle$.

### 2.3. *Quasiparticle-vibration couplings in the rotating frame*

For the description of rotational bands in odd-$A$ nuclei, it is always possible to adopt a basis constituted by one-quasiparticle excitations from rotational bands of even-even nuclei. Namely, the basic state vectors of the rotating shell model can be always written in the form $a_\mu^\dagger|\phi_{\rm band}\rangle$, where the quasiparticle operators and their vacuum $|\phi_{\rm band}\rangle$ are defined by Eq. (2.19). We now consider the couplings between the quasiparticles $a_\mu^\dagger$ and the RPA normal modes $X_n^{(\pm)\dagger}$ defined by Eq. (2.21) with respect to the rotational bands in even-even nuclei (see Fig. 1). Following essentially the same procedure as in the well-known



Fig. 1. Diagrammatic illustrations of the couplings between the quasiparticles (solid lines) and the generalized-gamma vibrations (wavy lines). The signatures $\alpha$ of these modes are indicated.

quasiparticle-vibration coupling models for non-rotating nuclei,[1],[2] we can derive from the original Hamiltonian, $\hat{H}'=\hat{h}'_{\rm sp}+\hat{H}_{\rm int}$, an effective Hamiltonian for odd-$A$ nuclei in the rotating frame:

$$\hat{H}_{\rm odd} = {\rm const} + \sum_\mu E_\mu a_\mu^\dagger a_\mu + \sum_{\bar{\mu}} E_{\bar{\mu}} a_{\bar{\mu}}^\dagger a_{\bar{\mu}}$$

$$+ \sum_n \hbar\omega_n^{(+)} X_n^{(+)\dagger} X_n^{(+)} + \sum_n \hbar\omega_n^{(-)} X_n^{(-)\dagger} X_n^{(-)} + \hat{H}_{\rm coupl}, \tag{2.22}$$

where*)

$$\hat{H}_{\rm coupl} = \sum_n \sideset{}{''}\sum_{\mu\nu} \Lambda_n^{(+)}(\mu\nu)(X_n^{(+)\dagger} a_\mu^\dagger a_\nu + X_n^{(+)} a_\nu^\dagger a_\mu)$$

$$+ \sum_n \sum_{\mu\bar{\nu}} \Lambda_n^{(-)}(\mu\bar{\nu})(X_n^{(-)\dagger} a_\mu^\dagger a_{\bar{\nu}} + X_n^{(-)} a_{\bar{\nu}}^\dagger a_\mu)$$

$$+ \sum_n \sum_{\mu\bar{\nu}} \Lambda_n^{(-)}(\bar{\nu}\mu)(X_n^{(-)\dagger} a_{\bar{\nu}}^\dagger a_\mu + X_n^{(-)} a_\mu^\dagger a_{\bar{\nu}}). \tag{2.23}$$

---

*) The double primes attached to $\sum$ denote that when the component $(\mu\nu)$ is summed, its signature partner $(\bar{\mu}\bar{\nu})$ should also be summed.

Explicit expressions for the quasiparticle-vibration-coupling vertices $\Lambda_n^{(\pm)}$ are

$$\Lambda_n^{(+)}(\mu\nu) = -\sum_{K=0,1,2}(-1)^K \kappa_K^{(+)} Q_K^{(+)}(n) Q_K^{(+)}(\mu\nu) ,$$

$$\Lambda_n^{(-)}(\mu\bar{\nu}) = \sum_{K=1,2}(-1)^K \kappa_K^{(-)} Q_K^{(-)}(n) Q_K^{(-)}(\mu\bar{\nu}) ,$$

$$\Lambda_n^{(-)}(\bar{\nu}\mu) = -\sum_{K=1,2} \kappa_K^{(-)} Q_K^{(-)}(n) Q_K^{(-)}(\mu\bar{\nu}) , \qquad (2\cdot24)$$

where $Q_K^{(\pm)}(n)$ are the quadrupole transition amplitudes associated with the vibrational modes $X_n^{(\pm)}$ and are given by

$$Q_K^{(+)}(n) = \sum_{\mu\bar{\nu}}\{\psi_n^{(+)}(\mu\bar{\nu}) Q_K^{(+)}(\mu\bar{\nu}) - (-1)^K \varphi_n^{(+)}(\mu\bar{\nu}) Q_K^{(+)}(\mu\bar{\nu})\} ,$$

$$Q_K^{(-)}(n) = \sum_{\mu<\nu}''\{\psi_n^{(-)}(\mu\nu) Q_K^{(-)}(\mu\nu) + (-1)^K \varphi_n^{(-)}(\mu\nu) Q_K^{(-)}(\mu\nu)\} . \qquad (2\cdot25)$$

In the above equations, $Q_K^{(\pm)}(\mu\nu)$ and $Q_K^{(\pm)}(\mu\bar{\nu})$ are the quasiparticle matrix elements of the (doubly-stretched) quadrupole operators $\tilde{Q}_K^{(\pm)}$ and are defined as

$$\tilde{Q}_K^{(\pm)} = \hat{Q}_K^{(\pm A)} + \hat{Q}_K^{(\pm B)} , \qquad (2\cdot26)$$

$$\left.\begin{array}{l} \hat{Q}_K^{(+A)} = \sum_{\mu\bar{\nu}} Q_K^{(+)}(\mu\bar{\nu})(A_{\mu\bar{\nu}}^\dagger + (-1)^K A_{\mu\bar{\nu}}) , \\[2mm] \hat{Q}_K^{(-A)} = \sum_{\mu<\nu}'' Q_K^{(-)}(\mu\nu)(A_{\mu\nu}^\dagger - (-1)^K A_{\mu\nu}) , \end{array}\right\} \qquad (2\cdot27)$$

$$\left.\begin{array}{l} \hat{Q}_K^{(+B)} = \sum_{\mu\nu}'' Q_K^{(+)}(\mu\nu) B_{\mu\nu}^\dagger , \\[2mm] \hat{Q}_K^{(-B)} = \sum_{\mu\bar{\nu}} Q_K^{(-)}(\mu\bar{\nu})(B_{\mu\bar{\nu}}^\dagger - (-1)^K B_{\mu\bar{\nu}}) , \end{array}\right\} \qquad (2\cdot28)$$

where

$$A_{\mu\nu}^\dagger = a_\mu^\dagger a_\nu^\dagger , \qquad B_{\mu\nu}^\dagger = a_\mu^\dagger a_\nu , \quad \text{etc} . \qquad (2\cdot29)$$

We note that the operators $\hat{Q}_K^{(\pm A)}$ can be rewritten in terms of the RPA normal modes as follows:

$$\hat{Q}_K^{(\pm A)} = \sum_n \{Q_K^{(\pm)}(n) X_n^{(\pm)\dagger} \pm (-1)^K Q_K^{(\pm)}(n) X_n^{(\pm)}\} \qquad (2\cdot30)$$

with $Q_K^{(\pm)}(n)$ being defined by Eq. $(2\cdot25)$ above. The quasiparticle-vibration-coupling Hamiltonian $\hat{H}_{\text{coupl}}$ has been derived from the cross terms between the above $\hat{Q}_K^{(\pm A)}$ parts and the $\hat{Q}_K^{(\pm B)}$ parts of the quadrupole operators $(2\cdot26)$ when they are inserted into the quadrupole-quadrupole interaction $(2\cdot18)$. In fact, there are contributions to the coupling vertices $(2\cdot24)$ also from the residual pairing interaction $(2\cdot17)$. Although we actually take into account these contributions in this work, they are omitted in the expression $(2\cdot24)$ since they are not important for the generalized-gamma vibrations on which we focus our attention hereafter.

   The quantities $(E_\mu, \hbar\omega_n^{(\pm)}, \Lambda_n^{(\pm)})$ and the operators $(a_\mu, X_n^{(\pm)})$ appearing in the above equations are defined with respect to a given band $|\phi_{\text{band}}\rangle$, and are functions of $\omega_{\text{rot}}$. It is important to notice that $\Lambda_n^{(-)}(\bar{\nu}\mu) \neq \Lambda_n^{(-)}(\mu\bar{\nu})$.

In this paper, we are particularly interested in the couplings to the generalized-gamma vibrations that evolve from the ordinary gamma vibrations (built on the ground states). Due to the effects of the triaxiality of the static single-particle potential and also due to the Coriolis couplings in the rotating frame, the generalized-gamma vibrations do not have definite $K$ quantum number but still contain the $|K|=2$ components as the largest components in the angular-momentum region investigated here. Neglecting the other vibrational modes and denoting the generalized-gamma vibrational modes with the signatures $\alpha=0$ $(r=+1)$ and $\alpha=1$ $(r=-1)$ as $X_r^\dagger$ and $X_{\bar r}^\dagger$, respectively, the internal state vectors of odd-$A$ nuclei can be written as superpositions of the quasiparticle and the generalized-gamma vibrational excitations:

$$|\chi_n(\omega_{\rm rot})\rangle = \sum_\mu \psi_n^{(1)}(\mu) a_\mu^\dagger |\phi\rangle$$

$$+ \sum_\mu \psi_n^{(3)}(\mu\gamma) a_\mu^\dagger X_r^\dagger |\phi\rangle + \sum_{\bar\mu} \psi_n^{(3)}(\bar\mu\,\bar\gamma) a_{\bar\mu}^\dagger X_{\bar r}^\dagger |\phi\rangle$$

$$+ \sum_\mu \psi_n^{(5)}(\mu\gamma\gamma) \frac{1}{\sqrt{2}} a_\mu^\dagger X_r^\dagger X_r^\dagger |\phi\rangle + \sum_\mu \psi_n^{(5)}(\mu\,\bar\gamma\,\bar\gamma) \frac{1}{\sqrt{2}} a_\mu^\dagger X_{\bar r}^\dagger X_{\bar r}^\dagger |\phi\rangle$$

$$+ \sum_{\bar\mu} \psi_n^{(5)}(\bar\mu\gamma\,\bar\gamma) a_{\bar\mu}^\dagger X_r^\dagger X_{\bar r}^\dagger |\phi\rangle$$

$$\text{for the } \alpha=1/2 \ (r=-i) \text{ sector ,} \tag{2.31}$$

where the generalized-gamma vibrations are taken into account up to double excitations. The internal state vectors for the $\alpha=-1/2(r=+i)$ sector take a form similar to above, except that the suffices $\mu$ are to be replaced by $\bar\mu$. The amplitudes $\psi_n^{(1)}(\mu)$, $\psi_n^{(3)}(\mu\gamma)$, etc. are determined by treating the quasiparticle and the vibrational modes as fermions and bosons, respectively, and by diagonalizing the Hamiltonian (2.22) in the model space (2.31). The diagonalization is carried out for each signature sector $(\alpha=+1/2$ and $-1/2)$ separately.

It is important to note that the state vector (2.31) contains, in general, many quasiparticles that are defined with respect to the yrast configuration, i.e., the quasiparticles $(\mathring{a}_\mu^\dagger, \mathring{a}_\nu^\dagger)$. For instance, it contains three such quasiparticles when the $s$-band (which involves two quasiparticle excitations from the $g$-band) is adopted as the vacuum $|\phi_{\rm band}\rangle$ for the quasiparticles $(a_\mu^\dagger, a_\nu^\dagger)$. When we discuss experimental data in § 4, we use the familiar terms like one-quasiparticle (1qp) bands and three-quasiparticle (3qp) bands by counting the number of quasiparticles defined with respect to the $g$-band before the first band crossing.

## 2.4. *Microscopic expressions for the intrinsic E2 and M1 operators*

In the previous subsection, we constructed the internal wave functions defined in the rotating frame. In order to calculate the $E2$ and $M1$ transition probabilities, however, we have to construct the total wave functions defined in the laboratory frame. We do this in a manner similar to the familiar particle-rotor model. Namely, we construct the state vectors in the laboratory frame in a direct product form of the rotational $D$-function $|IMK\rangle$ and the internal wave function $|\chi_n(\omega_{\rm rot})\rangle$:

$$|\Psi_{nIM\kappa}(\omega_{\rm rot})\rangle = |IM\kappa\rangle \otimes |\chi_n(\omega_{\rm rot})\rangle . \tag{2.32}$$

Note, however, that the projection $\kappa$ is defined here with respect to the $x$-axis which coincides with the rotation axis in the rotating shell model.

It is convenient to adopt the Holstein-Primakoff-type boson representation for the $D$-functions, which were invented by Marshalek.[26] In this representation, for instance, the rotational $D$-functions $|IM\kappa\rangle$ can be written in the subspace $\kappa = I$ in the following simple form:

$$|II_0I\rangle = \frac{1}{\sqrt{2\pi}} e^{i(I-I_0)\Phi} \frac{1}{\sqrt{(I-I_0)!}} (b^\dagger)^{I-I_0} |I_0 I_0 I_0\rangle . \tag{2.33}$$

Here the boson operator $b^\dagger$ transfers $\Delta M = -1$ and the operator $e^{i\Phi}$ transfers $\Delta I = \Delta M = \Delta\kappa = +1$. The angular-momentum shift operator $\hat{I}_-^{\rm (lab)}$ with respect to the laboratory frame is expressed as

$$\hat{I}_-^{\rm (lab)} = \hat{I}_y^{\rm (lab)} - i\hat{I}_z^{\rm (lab)}$$

$$= b^\dagger \sqrt{2\hat{I} - b^\dagger b} \quad \text{with} \quad \hat{I} = I_0 - i\frac{\partial}{\partial\Phi} . \tag{2.34}$$

As is evident from the above expressions, the Holstein-Primakoff-type boson representation is suited to an expansion in terms of $1/I_0$.

It is here very important to distinguish three frames of reference; the laboratory (lab) frame, the principal axis (PA) frame and the uniformly rotating (UR) frame.[27] They are related by

$$\hat{O}_{\lambda\mu}^{\rm (lab)} = e^{i\mu\Phi} \hat{O}_{\lambda\mu}^{\rm (UR)} = \sum_\kappa \hat{D}_{\mu\kappa}^\lambda \hat{O}_{\lambda\kappa}^{\rm (PA)} , \tag{2.35}$$

where $\hat{O}_{\lambda\mu}^{\rm (lab)}$, $\hat{O}_{\lambda\mu}^{\rm (UR)}$ and $\hat{O}_{\lambda\kappa}^{\rm (PA)}$ are the tensor operators of rank $\lambda$ defined in the lab-, UR- and PA- frame, respectively. Thus, for instance, we have the following relations for the quadrupole operators:

$$\hat{Q}_{2-1}^{\rm (UR)} = e^{i\Phi} \hat{Q}_{2-1}^{\rm (lab)} = e^{i\Phi} \sum_\kappa \hat{D}_{-1\kappa}^2 \hat{Q}_{2\kappa}^{\rm (PA)} . \tag{2.36}$$

Expanding the $\hat{D}$-operator in terms of $1/I_0$ and retaining the terms up to the $I_0^{-1/2}$ order,[*] we obtain

$$\hat{Q}_{2-1}^{\rm (UR)} \approx \sqrt{\frac{3}{2}} \frac{\hat{I}_-^{\rm (UR)}}{I_0} \hat{Q}_{20}^{\rm (PA)} - \frac{\hat{I}_+^{\rm (UR)}}{I_0} \hat{Q}_{2-2}^{\rm (PA)} + \hat{Q}_{2-1}^{\rm (PA)} , \tag{2.37}$$

where

$$\hat{I}_\pm^{\rm (lab)} = e^{\pm i\Phi} \hat{I}_\pm^{\rm (UR)} . \tag{2.38}$$

In order to calculate the $E2$ transition probabilities, we need to know the microscopic expressions for the intrinsic operators $\hat{Q}_{20}^{\rm (PA)}$, $\hat{Q}_{2-2}^{\rm (PA)}$ and $\hat{Q}_{2-1}^{\rm (PA)}$ acting on the internal wave functions $|\chi_n(\omega_{\rm rot})\rangle$. For this aim, we extend Marshalek's treatment[20] of the

---

[*] Up to the order $I_0^{-1/2}$, they are given[20],[26] by

$$\hat{D}_{12}^2 \approx 0, \ \hat{D}_{11}^2 \approx 0, \ \hat{D}_{10}^2 \approx \sqrt{3/2} \cdot \hat{I}_-^{\rm (lab)}/I_0, \ \hat{D}_{1-1}^2 \approx e^{-i\Phi}, \ \hat{D}_{1-2}^2 \approx -e^{-2i\Phi} \hat{I}_+^{\rm (lab)}/I_0 .$$

"Nambu-Goldstone modes" ($\Gamma^\dagger$ and $\Gamma$) to odd-$A$ nuclei. These are the modes that reorient the angular momentum of the collective rotation:

$$\Gamma^\dagger = \frac{1}{\sqrt{2I_c}}\hat{J}_-^{(\mathrm{RPA})} = \frac{1}{\sqrt{2I_c}}(\hat{J}_y^{(\mathrm{RPA})} - i\hat{J}_z^{(\mathrm{RPA})}),\tag{2·39}$$

where $I_c = \langle \hat{J}_x \rangle$ and the superscript denotes that they are evaluated in the RPA.[*] Hereafter, the expectation values are taken with respect to the RPA vacuum $|\phi_{\mathrm{band}}\rangle$. These modes appear among the RPA normal modes. The quadrupole operator $\hat{Q}_{2-1}$ is then expressed in terms of the RPA normal modes $\{X_n^{(-)\dagger}, X_n^{(-)}, \Gamma^\dagger, \Gamma\}$ and the quasiparticle operators $(B_{\mu\bar{\nu}}^\dagger, B_{\mu\bar{\nu}})$ as follows:

$$\hat{Q}_{2-1}^{(\mathrm{RPA})} = \langle \hat{Q}_{20} \rangle \sqrt{\frac{3}{I_c}}\Gamma^\dagger - \langle \hat{Q}_{22} \rangle \sqrt{\frac{2}{I_c}}\Gamma + \hat{Q}_{2-1}^{(\mathrm{vib})} + \hat{Q}_{2-1}^{(\mathrm{qp})},\tag{2·40}$$

where $\hat{Q}_{2-1}^{(\mathrm{vib})}$ and $\hat{Q}_{2-1}^{(\mathrm{qp})}$ are the vibrational and quasiparticle terms, respectively,

$$\hat{Q}_{2-1}^{(\mathrm{vib})} = \sum_n \{Q_{-1}^{(\mathrm{UR})}(n)X_n^{(-)\dagger} + Q_{+1}^{(\mathrm{UR})}(n)X_n^{(-)}\},\tag{2·41}$$

$$\hat{Q}_{2-1}^{(\mathrm{qp})} = \sum_{\mu\bar{\nu}} \{Q_{-1}^{(\mathrm{qp})}(\mu\bar{\nu})B_{\mu\bar{\nu}}^\dagger + Q_{+1}^{(\mathrm{qp})}(\mu\bar{\nu})B_{\mu\bar{\nu}}\}\tag{2·42}$$

with

$$Q_{\pm1}^{(\mathrm{UR})}(n) = \frac{i}{\sqrt{2}}(Q_1^{(-)}(n) \pm Q_2^{(-)}(n)),\tag{2·43}$$

$$Q_{\pm1}^{(\mathrm{qp})}(\mu\bar{\nu}) = \frac{i}{\sqrt{2}}(Q_1^{(-)}(\mu\bar{\nu}) \pm Q_2^{(-)}(\mu\bar{\nu})).\tag{2·44}$$

The subscripts in the above notations refer to the $x$-axis except for $Q_{K=1,2}^{(-)}(n)$ and $Q_{K=1,2}^{(-)}(\mu\bar{\nu})$ where $K$ denotes the $z$-component. Marshalek discussed[20] a formal unitary transformation which replaces the "Nambu-Goldstone modes" ($\Gamma^\dagger, \Gamma$) with the exact angular-momentum operators $(\hat{I}_-, \hat{I}_+)/\sqrt{2I_c}$. Extending his argument to odd-$A$ nuclei, we now assume that the following replacements are possible:

$$\left.\begin{array}{l} \Gamma^\dagger \longrightarrow \dfrac{1}{\sqrt{2I_c}}(\hat{I}_-^{(\mathrm{UR})} - \hat{J}_-^{(\mathrm{qp})}),\\[2ex] \Gamma \longrightarrow \dfrac{1}{\sqrt{2I_c}}(\hat{I}_+^{(\mathrm{UR})} - \hat{J}_+^{(\mathrm{qp})}), \end{array}\right\}\tag{2·45}$$

where $\hat{J}_\pm^{(\mathrm{qp})}$ are the angular-momentum operators acting on the odd quasiparticles $(a_\mu^\dagger, a_{\bar{\nu}}^\dagger)$. A similar ansatz was previously adopted by Hara and Kusuno[28] for the case $\omega_{\mathrm{rot}} = 0$. Then, Eq. (2·40) may be rewritten as

---

[*] Note that $I_0$ for odd-$A$ nuclei differs from $I_c$ for even-even nuclei by $\langle \hat{J}_x^{(\mathrm{qp})} \rangle = I_0 - I_c$, which represents the contribution from the last odd quasiparticle. We assume that the difference is small in comparison with $I_0$ itself so that it is possible to expand the functions of $I_0$ in terms of $\langle \hat{J}_x^{(\mathrm{qp})} \rangle / I_c$.

$$\hat{Q}_{2-1}^{(RPA)} = \langle \hat{Q}_{20} \rangle \sqrt{\frac{3}{2}} \frac{1}{I_c} ( \hat{I}_{-}^{(UR)} - \hat{J}_{-}^{(qp)} ) - \langle \hat{Q}_{22} \rangle \frac{1}{I_c} ( \hat{I}_{+}^{(UR)} - \hat{J}_{+}^{(qp)} )$$

$$+ \hat{Q}_{2-1}^{(vib)} + \hat{Q}_{2-1}^{(qp)} . \tag{2.46}$$

We now require that the above $\hat{Q}_{2-1}^{(RPA)}$ should be equivalent to the $I_0^{-1/2}$ order approximation of $\hat{Q}_{2-1}^{(UR)}$, Eq. (2·37). It should be recalled here that our microscopic calculation is done in the UR frame and that the RPA takes into account the $I_c^{-1/2}$ order corrections to the independent-quasiparticle limit of the rotating shell model. By comparing the coefficients in Eqs. (2·37) and (2·46) of the angular-momentum operators $\hat{I}_{\pm}^{(UR)}$, we obtain the microscopic expressions in the RPA order for the intrinsic operators $\hat{Q}_{2\nu}^{(PA)}$ to be used in the expression (2·37) for $Q_{2-1}^{(UR)}$:

$$\hat{Q}_{20}^{(PA)} = \langle \hat{Q}_{20} \rangle ,$$

$$\hat{Q}_{2-2}^{(PA)} = \langle \hat{Q}_{22} \rangle ,$$

$$\hat{Q}_{2-1}^{(PA)} = \hat{Q}_{2-1}^{(vib)} + \hat{Q}_{2-1}^{(qp)} - \langle \hat{Q}_{20} \rangle \sqrt{\frac{3}{2}} \frac{1}{I_c} \hat{J}_{-}^{(qp)} + \langle \hat{Q}_{22} \rangle \frac{1}{I_c} \hat{J}_{+}^{(qp)} . \tag{2.47}$$

In the same way, we can derive the microscopic expressions for the intrinsic $M1$ operators $\hat{\mu}_{1\kappa}^{(PA)}$ defined by

$$\hat{\mu}_{1-1}^{(UR)} = e^{i\Phi} \hat{\mu}_{1-1}^{(lab)} = e^{i\Phi} \sum_{\kappa} \hat{D}_{-1\kappa}^{1} \hat{\mu}_{1\kappa}^{(PA)} . \tag{2.48}$$

Expanding the $\hat{D}$-operator in terms of $1/I_0$ and retaining the terms up to the $I_0^{-1/2}$ order,[*] we obtain

$$\hat{\mu}_{1-1}^{(UR)} \approx \hat{\mu}_{1-1}^{(PA)} + \frac{1}{\sqrt{2}} \frac{1}{I_0} \hat{I}_{-}^{(UR)} \hat{\mu}_{10}^{(PA)} . \tag{2.49}$$

On the other hand, the $M1$ operator $\hat{\mu}_{1-1}$ is represented by the RPA normal modes in the UR frame as

$$\hat{\mu}_{1-1}^{(RPA)} = \frac{1}{\sqrt{I_c}} \langle \hat{\mu}_x \rangle \Gamma^{\dagger} + \hat{\mu}_{1-1}^{(vib)} + \hat{\mu}_{1-1}^{(qp)} , \tag{2.50}$$

where $\hat{\mu}_{1-1}^{(vib)}$ and $\hat{\mu}_{1-1}^{(qp)}$ are the vibrational and quasiparticle terms, respectively,

$$\hat{\mu}_{1-1}^{(vib)} = \sum_{n} \{ \mu_{-1}^{(UR)}(n) X_n^{(-)\dagger} + \mu_{+1}^{(UR)}(n) X_n^{(-)} \} , \tag{2.51}$$

$$\hat{\mu}_{1-1}^{(qp)} = \sum_{\mu\bar{\nu}} \{ \mu_{-1}^{(qp)}(\mu\bar{\nu}) B_{\mu\bar{\nu}}^{\dagger} + \mu_{+1}^{(qp)}(\mu\bar{\nu}) B_{\mu\bar{\nu}} \} \tag{2.52}$$

with

$$\mu_{-1}^{(UR)}(n) = \langle [X_n^{(-)}, \hat{\mu}_{1-1}] \rangle ,$$

$$\mu_{+1}^{(UR)}(n) = \langle [\hat{\mu}_{1-1}, X_n^{(-)\dagger}] \rangle . \tag{2.53}$$

As before, the components of $\hat{\mu}$ refer to the $x$-axis. In deriving Eq. (2·50), we have

---

[*] Up to the order $I_0^{-1/2}$, they are given[20],[26] by

$$\hat{D}_{-11}^{1} \approx 0, \quad \hat{D}_{-10}^{1} \approx \hat{I}_{-}^{(lab)}/\sqrt{2I_0} , \quad \hat{D}_{-1-1}^{1} \approx e^{-i\Phi} .$$

used the identity $\langle \hat{\mu}_x \rangle / \sqrt{I_c} = \langle [\Gamma, \hat{\mu}_{1-1}] \rangle$. Following the prescription (2·45) for the replacement of the "Nambu-Goldstone modes", we can rewrite Eq. (2·50) as

$$\hat{\mu}_{1-1}^{(\mathrm{RPA})} = \frac{1}{\sqrt{2}} \langle \hat{\mu}_x \rangle \frac{1}{I_c} ( \hat{I}_-^{(\mathrm{UR})} - \hat{J}_-^{(\mathrm{qp})} ) + \hat{\mu}_{1-1}^{(\mathrm{vib})} + \hat{\mu}_{1-1}^{(\mathrm{qp})} . \tag{2·54}$$

Requiring that the above $\hat{\mu}_{1-1}^{(\mathrm{RPA})}$ should be equivalent to the $I_0^{-1/2}$-order approximation of $\hat{\mu}_{1-1}^{(\mathrm{UR})}$, Eq. (2·49), we obtain

$$\hat{\mu}_{10}^{(\mathrm{PA})} = \langle \hat{\mu}_x \rangle ,$$

$$\hat{\mu}_{1-1}^{(\mathrm{PA})} = \hat{\mu}_{1-1}^{(\mathrm{vib})} + \hat{\mu}_{1-1}^{(\mathrm{qp})} - g_{\mathrm{RPA}} \hat{J}_{-1}^{(\mathrm{qp})} , \tag{2·55}$$

where

$$g_{\mathrm{RPA}} = \langle \hat{\mu}_x \rangle / I_c \tag{2·56}$$

and $\hat{J}_{-1}^{(\mathrm{qp})} = \hat{J}_-^{(\mathrm{qp})} / \sqrt{2}$. Microscopic expressions in the RPA order for other components of the $E2$ and $M1$ operators, $\hat{Q}_{2\mu}$ and $\hat{\mu}_{1\mu}$, can be obtained in a similar manner.

After obtaining the explicit expressions for the intrinsic operators, it is straightforward to calculate the $B(M1)$ and $B(E2)$ values by using the total wave function defined by Eq. (2·32) with $\kappa = I$.

### 2.5. *Effects of triaxial deformations on $B(E2; I \rightarrow I-1)$*

In this subsection, we discuss the effects of triaxial deformations on the $B(E2; I \rightarrow I-1)$ values between the signature partners in the odd-$A$, unique-parity bands. As is evident from the expressions (2·36) and (2·37), the intrinsic operator $\hat{Q}_{2-1}^{(\mathrm{PA})}$ is responsible for such signature-changing transitions with $\Delta I = 1$. Let us rewrite this operator into a form, by means of which we can easily identify the effects of static triaxial deformation on the $E2$ transitions. Expressing the expectation values of the quadrupole operators $\langle \hat{Q}_{20} \rangle$ and $\langle \hat{Q}_{22} \rangle$ in terms of $Q_0 \equiv \langle \hat{Q}_{K=0}^{(+)} \rangle$ and $Q_2 \equiv \langle \hat{Q}_{K=2}^{(+)} \rangle / \sqrt{2}$, whose components are defined with respect to the $z$-axis, and using $\hat{J}_{\pm}^{(\mathrm{qp})} = \hat{J}_y^{(\mathrm{qp})} \pm i \hat{J}_z^{(\mathrm{qp})}$, the intrinsic operator $\hat{Q}_{2-1}^{(\mathrm{PA})}$ in Eq. (2·47) is rewritten as

$$\frac{1}{i} \hat{Q}_{2-1}^{(\mathrm{PA})} = \frac{1}{i} \hat{Q}_{2-1}^{(\mathrm{vib})} + \frac{1}{i} \hat{Q}_{2-1}^{(\mathrm{qp})} - \sqrt{\frac{3}{2}} Q_0 \frac{\hat{J}_z^{(\mathrm{qp})}}{I_c} + Q_2 \left( 2 \frac{i \hat{J}_y^{(\mathrm{qp})}}{I_c} + \frac{\hat{J}_z^{(\mathrm{qp})}}{I_c} \right) . \tag{2·57}$$

We can eliminate $i\hat{J}_y^{(\mathrm{qp})}$ from the above expression by making use of the approximate relation

$$i \hat{J}_y^{(\mathrm{qp})} \approx (-1)^{I_i - j} \frac{|\Delta E|}{\hbar \omega_{\mathrm{rot}}} \hat{J}_z^{(\mathrm{qp})} , \tag{2·58}$$

where $I_i$ denotes the angular-momentum of the initial state. Here $\Delta E$ is defined by $\Delta E = E(\alpha = 1/2) - E(\alpha = -1/2)$ and represents the signature splitting of the quasiparticle energies associated with the unique-parity orbit $j$. The phase factor $(-1)^{I_i - j}$ in the above relation is obtained by assuming the normal phase rule $\Delta E = (-1)^{j+1/2} |\Delta E|$, and implies that it is positive (negative) for the transitions from the favoured (unfavoured) states whose angular-momentum $I_i = j + \mathrm{even}$ (odd). The relation (2·58)

is easily derived[14] by taking the quasiparticle matrix elements of the commutator between the cranking Hamiltonian $\hat{h}'_{sp} = \hat{h}_{sp} - \omega_{rot}\hat{J}_x$ and the operator $\hat{J}_z$, and holds almost exactly in the axial symmetric limit except for the small corrections resulting from the doubly stretched $l^2$ and $l \cdot s$ terms. Inserting (2·58) into (2·57), we obtain

$$\frac{1}{i}\hat{Q}_{2-1}^{(PA)} = \frac{1}{i}\hat{Q}_{2-1}^{(vib)} + \frac{1}{i}\hat{Q}_{2-1}^{(qp)} + \left\{ -\sqrt{\frac{3}{2}}Q_0 + Q_2\left(1 + 2(-1)^{I_i-j}\left|\frac{\Delta E}{\hbar\omega_{rot}}\right|\right)\right\}\frac{\hat{J}_z^{(qp)}}{I_c}.$$

(2·59)

The above expression clearly shows that the signature dependent effect arises when the static triaxiality $Q_2$ is non-zero. The phase factor $(-1)^{I_i-j}$ implies that the $B(E2; I_i \to I_i - 1)$ values are enhanced for the transitions from the favoured (unfavoured) states to the unfavoured (favoured) states when $Q_2$ is negative (positive). According to Bohr and Mottelson's definitions[3] of $\gamma_0$, i.e., $\tan\gamma_0 \equiv \langle\hat{Q}_{K=2}^{(+)}\rangle/\langle\hat{Q}_{K=0}^{(+)}\rangle$, $\gamma_0$ is positive (negative) when $Q_2$ is positive (negative). Note that this sign convention for $\gamma_0$ is opposite to that of the Lund convention.[14] If the vibrational and the quasiparticle contributions, $\hat{Q}_{2-1}^{(vib)}$ and $\hat{Q}_{2-1}^{(qp)}$, are neglected, Eq. (2·59) reduces to the expression derived by Hamamoto and Mottelson[14],[15] when $j = 1/2$ because $|\Delta E| = \hbar\omega_{rot}$ in this special case.

In addition to the static triaxial deformation $Q_2 \neq 0$, the vibrational term $\hat{Q}_{2-1}^{(vib)}$ also brings about signature dependent effects in the $B(E2; I \to I-1)$. This is caused by the mixings of the generalized-gamma vibration with signature $\alpha = 1$ ($r = -1$) in the one-quasiparticle states, illustrated in Fig. 1(a). Microscopic structure of the coupling vertices $\Lambda_n^{(\pm)}$ appearing in Fig. 1 and defined by Eq. (2·24) will be investigated in detail in a separate paper.[29] We here only mention that they involve the matrix elements of $\hat{Q}_{K=1}^{(-)}$ and $\hat{Q}_{K=2}^{(-)}$ between the aligned quasiparticle states with different signatures, for which an approximate relation

$$\hat{Q}_{K=2}^{(-)(qp)} \approx -(-1)^{I_i-j}\frac{|\Delta E|}{\hbar\omega_{rot}}\hat{Q}_{K=1}^{(-)(qp)}$$

(2·60)

holds under certain conditions. The above relation plays a role similar to the relation (2·58) between $i\hat{J}_y^{(qp)}$ and $\hat{J}_z^{(qp)}$ in deriving a phase rule for the signature dependent effects. It should be emphasized here that such an interplay between the $K = 1$ and 2 components of the quadrupole motion is an interesting new feature of the generalized-gamma vibrations created in rotating triaxial nuclei.[30]

Thus, we expect in general that the signature dependence of $B(E2; I \to I-1)$ is very sensitive to whether effects of static and dynamic gamma deformations result in constructive coherence or destructive coherence. The degree of the competition (or the cooperation) between the static and dynamic effects depends, of course, on the magnitude of the $\gamma_0$ and the strengths of the quasiparticle-vibration-coupling vertices $\Lambda^{(-)}$.

### 2.6. *Effects of aligned quasiparticles on B(M1)*

The intrinsic operator $\bar{\mu}_{-1}^{(PA)}$ defined by Eq. (2·55) is responsible for the $M1$ transitions between the signature-partner bands. This operator may be rewritten as

$$\hat{\mu}_{1-1}^{(PA)} = (g_l - g_{RPA}) \hat{l}_{-1}^{(qp)} + (g_s - g_{RPA}) \hat{s}_{-1}^{(qp)} + \hat{\mu}_{1-1}^{(vib)}, \tag{2.61}$$

in terms of the expressions $\hat{\mu}_{1-1}^{(qp)} = g_l \hat{l}_{-1}^{(qp)} + g_s^{eff} \hat{s}_{-1}^{(qp)}$ and $\hat{J}_{-1}^{(qp)} = \hat{l}_{-1}^{(qp)} + \hat{s}_{-1}^{(qp)}$. The $g$-factor of the RPA vacuum, $g_{RPA}$, appearing in the above equation is defined by Eq. (2.56) and may be rewritten into a more explicit form,[31)~33)]

$$g_{RPA} = g_R + (g_i - g_R) \frac{i}{R+i}, \tag{2.62}$$

where $R \equiv \langle \hat{J}_x \rangle_g$, $i \equiv \langle \hat{J}_x \rangle - \langle \hat{J}_x \rangle_g$, $g_R R \equiv \langle \hat{\mu}_x \rangle_g$ and $g_i i \equiv \langle \hat{\mu}_x \rangle - \langle \hat{\mu}_x \rangle_g$, with the suffix $g$ denoting the expectation value with respect to the $g$-band configuration. We see from the expression (2.62) that $g_{RPA}$ decreases (increases) when the $i_{13/2}$ neutron ($h_{11/2}$ proton) alignment takes place, since $g_i$ is negative (positive) in this case. This change in the $g_{RPA}$ value associated with the alignment will, in turn, bring about a remarkable change in the $M1$ transition probabilities under consideration. Thus, in the case of odd-$Z$ nuclei with the $h_{11/2}$ odd proton, the $B(M1)$ values will increase (decrease) when one goes from the 1qp band to the 3qp band involving the aligned $i_{13/2}$ neutrons ($h_{11/2}$ protons). On the other hand, for odd-$N$ nuclei with the $i_{13/2}$ odd neutron, the $B(M1)$ values will increase (decrease) when the $h_{11/2}$ proton ($i_{13/2}$ neutron) alignment takes place.

## § 3. Details of numerical calculation

The procedure of numerical calculation is basically the same as in Ref. 17) except that the new method of constructing the diabatic quasiparticle representation[22),23)] is used for the first time in this work. We adopt the second-order approximation with respect to the power of the $\omega_{rot}$ expansion for determining the operator $iG$ in Eq. (2.5). The parameters $v_{ls}$ and $v_{ll}$ of the modified-harmonic-oscillator potential are taken from Bohr and Mottelson's textbook.[3)] The three major shells with $N_{osc} = 3, 4, 5$ ($N_{osc} = 4, 5, 6$) are explicitly taken into accont for protons (neutrons),[*)] and the $\Delta N_{osc} = 2$ Coriolis coupling terms are neglected in the calculation. The equilibrium deformation parameters ($\beta_0, \gamma_0$) are determined by using the same method as in Ref. 25).[*)] This method makes use of the semiclassical requirement that the velocity distribution should be isotropic in average when seen in the rotating frame.

The pairing-force strengths used are $G_n = 2.64/A$ and $G_P = 3.51/A$ in units of $\hbar\omega_0$. These values are determined by the requirement that the calculated pairing gaps at $\hbar\omega_{rot} = 0$ reproduce the odd-even mass differences between $^{165}$Lu and its even-even neighbours. The pairing gaps $\Delta_n$ and $\Delta_p$ are selfconsistently calculated as functions of $\omega_{rot}$ in each quasiparticle configuration for even-even nuclei. It turned out, however, that the $\Delta_n$ for the $s$-band configuration rapidly decreases in the region $\hbar\omega_{rot} \gtrsim 0.3$ MeV. In such a case, we simply set the pairing gaps to be constant in such a region in order to avoid the difficulty associated with the pairing phase transition. These constant values are shown by thin dash-dotted lines in Fig. 4.

The quadrupole-force strengths $\kappa_K^{(\pm)}$ are determined in the following way. In the

---

[*)] The contributions from the nucleons outside the model space are taken into account in the same way as in Ref. 25). They are indispensable for reproducing the experimental data for $\beta_0$ in the calculations.

RPA calculation for the vibrations built on the $g$-band, we determine the values of $\kappa_0^{(+)}$ and $\kappa_2^{(+)}$ in each nucleus so as to reproduce at $\hbar\omega_{\mathrm{rot}}=0$ the average excitation energies of the lowest $K=0$ and 2 vibrational states in the neighbouring even-even nuclei. On the other hand, the values of $\kappa_1^{(\pm)}$ and $\kappa_2^{(-)}$ are determined at $\hbar\omega_{\mathrm{rot}}=0$ so as to restore in the RPA the rotational symmetry broken by the deformed single-particle potential $\hat{h}_{\mathrm{def}}$. Since the equilibrium deformation parameters $(\beta_0, \gamma_0)$ are different between the $g$-band and the $s$-band configurations, the strengths $\kappa_K^{(\pm)}$ of the residual quadrupole-force are also slightly different between these configurations. In the RPA calculation for the vibrations built on the $s$-band, we assume, for simplicity, that $\kappa_0^{(+)}=\kappa_1^{(\pm)}=\kappa_2^{(\pm)}=\kappa$ and determine the value of $\kappa$ at $\hbar\omega_{\mathrm{rot}}=0.2\,\mathrm{MeV}$ such that the excitation energy $\hbar\omega_{\mathrm{NG}}$ of the "Nambu-Goldstone mode" (that reorients the angular momentum of the collective rotation) is correctly reproduced in the calculation at $\hbar\omega_{\mathrm{NG}}=\hbar\omega_{\mathrm{rot}}$.

In the treatment of the quasiparticle-vibration couplings, we take into account the lowest 10 quasiparticle states (with unique-parity) for each signature sector, $\alpha=\pm 1/2$. Thus, we diagonalize the $60\times 60$ matrix for each signature at every value of $\omega_{\mathrm{rot}}$.

The $M1$ and $E2$ transition matrix elements are evaluated at the average value of $\omega_{\mathrm{rot}}$'s between the initial and the final states.[*] In the calculation, the effective spin $g$-factor of $g_s^{\mathrm{eff}}=0.7g_s^{\mathrm{free}}$ is used, but no $E2$ effective charge is used. The rotational $g$-factor, $g_R$, appearing in Eq. (2·62) is usually calculated in a microscopic way. However, for the cases where it is apparent that a better agreement between calculated results and experimental data is obtainable if we phenomenologically modify the $g_R$ value, we shall present the results of calculation using the phenomenological $g_R$ values. These cases occur in nuclei involving the $i_{13/2}$ odd neutrons, and are explicitly mentioned in §4.

It should be emphasized that we are going to do calculations which essentially contain no adjustable parameter. Since our major purpose in this paper is to examine the general characteristics of the prediction of the microscopic model formulated in §2, we shall not attempt, except for a few cases mentioned above, in the next section to phenomenologically search for the optimal parameters entering in the numerical calculations. Of particular important one is the triaxiality parameter $\gamma_0$ characterizing the single-particle potential $\hat{h}_{\mathrm{def}}$. Since we use in this paper a very simple method of evaluating $\gamma_0$, there is room to improve the calculation especially with regard to the determination of the most appropriate values of $\gamma_0$ for individual bands. We leave such a task of elaborating our calculation in order to make a detailed comparison with experimental data for a future work.

## §4. Some examples of numerical calculation

In this section, we present some results of numerical calculation for the unique-parity bands of odd-$Z$ nuclei, $^{157}$Ho, $^{159}$Tm, $^{161,165}$Lu, and of odd-$N$ nuclei, $^{161}$Dy, $^{167}$Er and $^{161,163,167}$Yb for which experimental data for $B(M1)$ and/or $B(E2)$ are available. Before presenting these results, we first test our theoretical values of $g_{\mathrm{RPA}}$ in $^{168}$W, since a result of direct measurement of the $g$-factors of both the $g$-band and the $s$-band has

---

[*] Since the wave functions in the diabatic basis change only smoothly as functions of $\omega_{\mathrm{rot}}$, we expect that this is a good approximation.

recently been reported[34] for the first time for this nucleus.

### 4.1. *g-factors of the g- and the s-band in $^{168}W$*

Calculated and experimental values of the $g$-factors for the $g$- and the $s$-band in $^{168}$W are compared in Fig. 2. As expected, the $g$-factor for the $s$-band suddenly decreases to about $-0.2$ due to the alignment of the $i_{13/2}$ neutrons. The calculation successfully reproduces this change in the $g$-factors before and after the band crossing. Equation $(2\cdot61)$ indicates that the $B(M1)$ values of odd-$A$ nuclei sensitively depend on the $g$-factors of the even-even "core". Thus, the agreement displayed in Fig. 2 is quite encouraging to proceed to the discussion on the $B(M1)$ and $B(E2)$ values in odd-$A$ nuclei.

### 4.2. *Nuclei with the $h_{11/2}$ odd-proton*

Figure 3 presents the deformation parameters $(\beta_0, \gamma_0)$ for the 1qp and 3qp bands in $^{157}$Ho, $^{159}$Tm and $^{161,165}$Lu. These deformation parameters are equivalent to the $(\beta^{(pot)}, \gamma^{(pot)})$ defined in Ref. 25) that characterize the deformed potential in $\hat{h}_{\mathrm{def}}$ for the even-even "cores" (the averages of the neighbouring even-even nuclei) of the odd-$Z$ nuclei under consideration. These values are calculated by means of the semiclassical method described in § 2, and are used in the quasiparticle-vibration coupling calculations for evaluating the $M1$ and $E2$
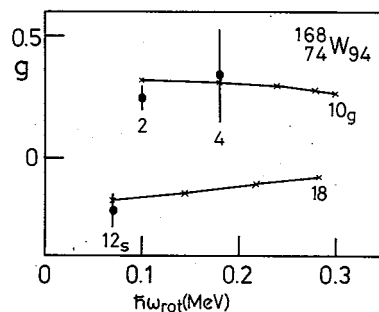


Fig. 2. Comparison of the calculated values of $g_{\mathrm{RPA}}$ with the corresponding experimental data[34] in $^{168}$W. The calculated deformation parameters $(\beta_0, \gamma_0)$ are $\beta_0 = 0.177 \sim 0.186$ and $\gamma_0 = 1.1° \sim 9.3°$ for the $g$-band, and $\beta_0 = 0.182 \sim 0.187$ and $\gamma_0 = 0.8° \sim 4.2°$ for the $s$-band, in the range $0.1 \lesssim \hbar\omega_{\mathrm{rot}} \lesssim 0.3$ MeV.
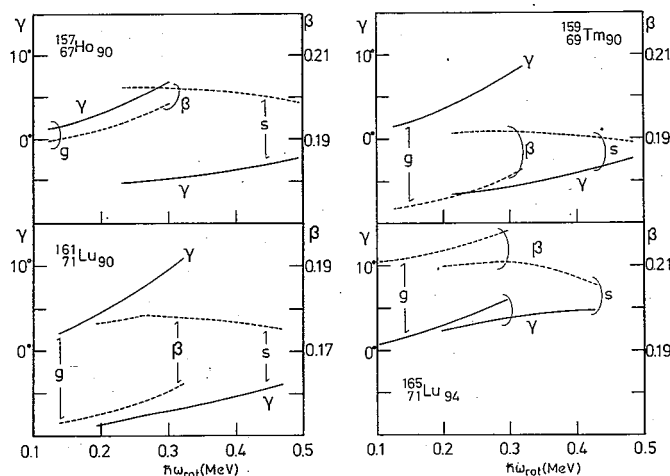


Fig. 3. Calculated deformation parameters $(\beta_0, \gamma_0)$ for the $g$-band and the $s$-band configuration are plotted as functions of $\omega_{\mathrm{rot}}$. These values characterize the deformation of the "cores" (the averages of the even-even neighbours) of the odd-$Z$ nuclei; $^{157}$Ho, $^{159}$Tm, $^{161}$Lu and $^{165}$Lu. Note that our definition of the sign of $\gamma_0$ is opposite to the Lund convention.[14]
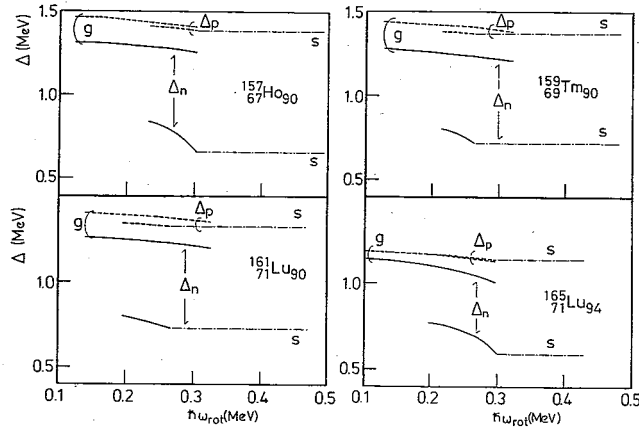
Fig. 4. Calculated pairing gaps $(\Delta_p, \Delta_n)$ for the $g$-band and the $s$-band configurations are plotted as functions of $\omega_{\text{rot}}$. These values characterize the pairing deformation of the "cores" (the averages of the even-even neighbours) of the odd-$Z$ nuclei; $^{157}$Ho, $^{159}$Tm, $^{161}$Lu and $^{165}$Lu.

transition properties within the unique-parity bands.

It is seen in Fig. 3 that the $\beta_0$ values do not significantly change when one goes from the $g$-band to the $s$-band. On the other hand, the sign of $\gamma_0$ changes, in the case of the $N=90$ isotones, from positive to negative due to the excitation of the aligned $i_{13/2}$ neutrons. (Note that our definition of the sign of $\gamma_0$ is opposite to the Lund convention[14]).

Results of the numerical calculation for the ratios $B(M1)/B(E2)$ in the $N=90$ isotones, $^{157}$Ho, $^{159}$Tm and $^{161}$Lu, with the $h_{11/2}$ odd-proton are displayed in Figs. 5~7. In these figures, the solid (broken) lines show the results of calculation in which the coupling effects with the generalized-gamma vibrations are taken into account (neglected). The solid triangles and the solid circles with error bars denote the experimental data before and after the first band crossings, respectively. In the upper parts of these figures, calculated values for the signature splittings $\Delta E$ of the quasiparticle energies are compared with the experimental data.

A remarkable feature of the observed $M1$ transition properties in these nuclei is that the $B(M1)$ values increase when one goes from the 1qp band to the 3qp band. The reason for this enhancement is easily understood from the expression (2·62): The $g$-factor associated with the aligned $i_{13/2}$ neutrons, $g_i$, is about $-0.18$ so that the $g_{\text{RPA}}$ values considerably decreases when one goes from the 1qp band to the 3qp band. This reduction of $g_{\text{RPA}}$, on the other hand, brings about an enhancement of the $B(M1)$ values under consideration, as is easily seen from the expression (2·61).

It is furthermore seen from Figs. 5~7 that the calculated values of the ratio $B(M1)/B(E2)$ for the 3qp bands increase as $Z$ increases from 67 to 71. There are two causes for this trend. One is the slight increase of the $B(M1)$ values associated with the decrease of the $g_{\text{RPA}}$ values; i.e., $g_{\text{RPA}} = -0.029$, $-0.045$ and $-0.062$ at $\hbar\omega_{\text{rot}}=0.4$ MeV for $^{157}$Ho, $^{159}$Tm and $^{161}$Lu, respectively. The other cause is the decrease of the $B(E2)$ values associated with the decrease of the deformation parameter $\beta_0$; i.e., $B(E2; I \rightarrow I-2) = 0.83$, 0.77 and 0.67 $[e^2b^2]$ at $\hbar\omega_{\text{rot}}=0.4$ MeV for $^{157}$Ho, $^{159}$Tm and $^{161}$Lu, respectively (see Fig. 3 for the $\beta_0$ values). The theoretical result that the ratio

$B(M1)/B(E2)$ in the $N=90$ isotones increases with increasing $Z$ is in agreement with the experiments. On the other hand, the theoretical pattern as a function of $\omega_{rot}$ is qualitatively similar for these isotopes, and do not explain the variations that are seen in the experimental data when one goes from one isotone to another.

As is well known,[14] the signature dependence of the $B(M1)$ is closely correlated with the signature splitting $\Delta E$ of the quasiparticle energies. On the other hand, this quantity $\Delta E$ is a rather sensitive function of the triaxiality parameter $\gamma_0$. Our $\gamma_0$ values used in Figs. 5~7 are qualitatively consistent with those evaluated by Frauendorf and May,[35] and by Hamamoto and Mottelson.[14] However, quantitatively, the absolute magnitudes of our $\gamma_0$ are much smaller than their values. As mentioned in §3, there is room for elaborating our calculation especially with respect to the determination of $\gamma_0$. For example, the polarization effects of the odd quasiparticle are not fully taken into account in the present calculation (since our $(\beta_0, \gamma_0)$ values are evaluated in the neighbouring even-even nuclei), although a part of such polarization effects may be taken into account in our model through the quasiparticle-vibration
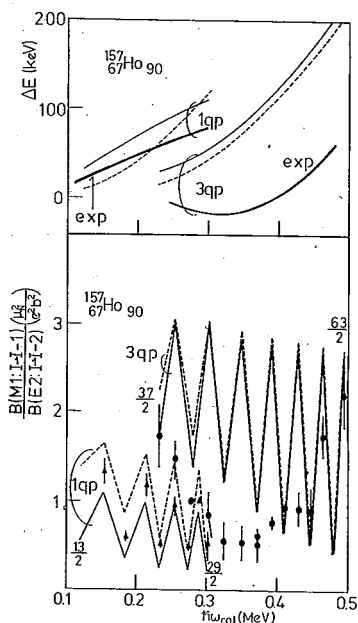


Fig. 5. Ratios $B(M1; I \rightarrow I-1)/B(E2; I \rightarrow I-2)$ and the signature splittings $\Delta E$ for $^{157}$Ho, plotted as functions of $\omega_{rot}$. The solid (broken) lines represent the results of calculation with (without) taking into account the couplings with the generalized-gamma vibrations. The solid triangles and the solid circles with error bars denote the experimental ratios[4],[8] before and after the first band crossings, respectively. The experimental data for the signature splitting $\Delta E$ are shown by the bold lines in the upper part of this figure, where all lines are drawn by smoothly interpolating the experimental and theoretical values.
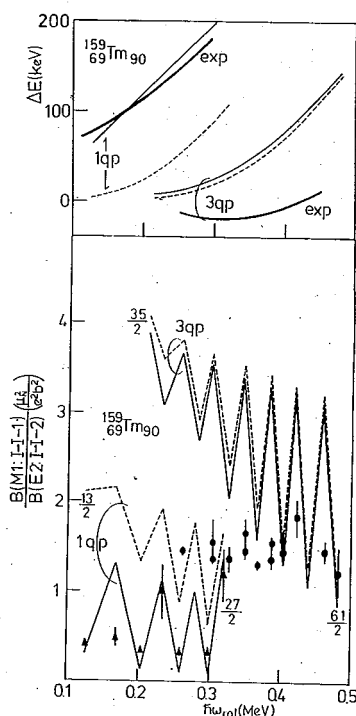
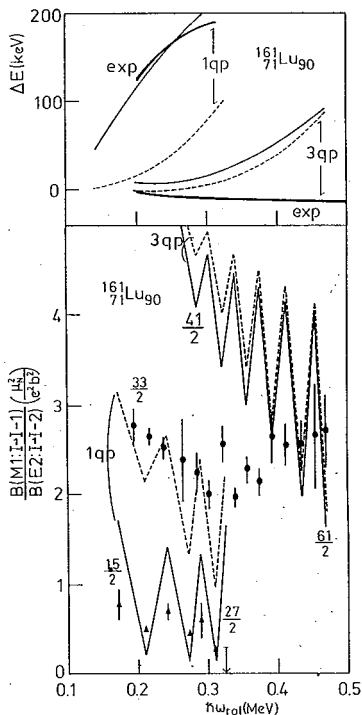Fig. 6. Same as Fig. 5 but for $^{159}$Tm. Experimental data are taken from Refs. 7) and 8).

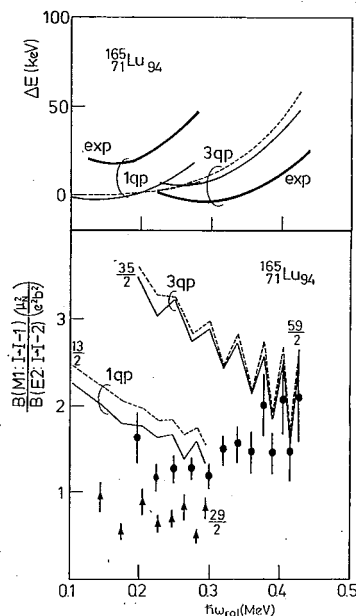Fig. 7. Same as Fig. 5 but for $^{161}$Lu. Experimental data are taken from Ref. 8).

Fig. 8. Same as Fig. 5 but for $^{165}$Lu. Experimental data are taken from Ref. 9). Note that the experimental data for $\hbar\omega_{\mathrm{rot}} \gtrsim 0.4$ MeV might correspond to the 5qp band.[9],[36]

couplings.

A similar theoretical pattern is also seen in $^{165}$Lu with $N = 94$ (see Fig. 8). In this nucleus, the magnitude of the ratios $B(M1; I \to I-1)/B(E2; I \to I-2)$ is somewhat overestimated. The calculated values for the collective $g$-factor, $g_R$ defined in Eq. (2·62), are $0.32 \sim 0.27$ in the range $0.1 \lesssim \hbar\omega_{\mathrm{rot}} \lesssim 0.3$ MeV. The experimental ratios can be reproduced, however, if we use the phenomenological value 0.4 adopted in Ref. 14) in place of the microscopically calculated $g_R$, except for the 3qp band in the region $0.2 \lesssim \hbar\omega_{\mathrm{rot}} \lesssim 0.3$ MeV where the experimental values are remarkably smaller than the calculated values. In this nucleus, it seems likely that the experimental data for $\hbar\omega_{\mathrm{rot}} \gtrsim 0.4$ MeV correspond to the $M1$ transitions associated with the 5qp band. This possibility was discussed in Ref. 9) and in our previous paper.[36]

It is seen from Figs. 5~8 that the main effect of the couplings with the generalized-gamma vibrations on the $M1$ transition properties is to decrease the magnitudes of the $B(M1)$ values to some extent. A direct origin of this reduction is that the 1qp amplitude $\psi_n^{(1)}(\mu)$ in Eq. (2·31) becomes less than one due to the coupling effects. This reduction effect is found to be stronger in the 1qp band than in the 3qp band. Some numerical examples for the amplitudes characterizing the internal wave function defined by Eq. (2·31) are presented in Table I.

Calculated $E2$ transition rates for $^{157}$Ho and $^{159}$Tm are presented in Figs. 9 and 10, respectively. Comparing the solid lines (in which the coupling effects of the generalized-gamma vibrations are taken into account) with the broken lines (where

Table I. Calculated values for the amplitudes of the internal wave functions, defined by Eq. (2·31), valid for the 1qp and the 3qp band at $\hbar\omega_{rot}=0.26$ MeV in $^{159}$Tm. Only the major amplitudes (among the 60 components) are listed.

| amplitudes | 1qp band | | 3qp band | |
|---|---|---|---|---|
| | $\alpha=1/2$ (unfavored) | $\alpha=-1/2$ (favored) | $\alpha=1/2$ (unfavored) | $\alpha=-1/2$ (favored) |
| $\phi^{(1)}(\mu)$ or $\phi^{(1)}(\bar\mu)$ | 0.889 | 0.780 | 0.989 | 0.992 |
| $\phi^{(3)}(\mu\gamma)$ or $\phi^{(3)}(\bar\mu\gamma)$ | 0.141 | 0.416 | −0.010 | −0.014 |
| $\phi^{(3)}(\bar\mu\bar\gamma)$ or $\phi^{(3)}(\mu\bar\gamma)$ | −0.250 | 0.048 | 0.110 | 0.092 |
| $\phi^{(5)}(\mu\gamma\gamma)$ or $\phi^{(5)}(\bar\mu\gamma\gamma)$ | 0.019 | 0.175 | −0.003 | −0.003 |
| $\phi^{(5)}(\mu\bar\gamma\bar\gamma)$ or $\phi^{(5)}(\bar\mu\bar\gamma\bar\gamma)$ | −0.045 | −0.007 | 0.015 | 0.012 |
| $\phi^{(5)}(\bar\mu\gamma\bar\gamma)$ or $\phi^{(5)}(\mu\gamma\bar\gamma)$ | −0.110 | 0.034 | 0.001 | 0.001 |

these effects are neglected), we see a drastic effect of the generalized-gamma vibrations on the $B(E2)$ values with $\Delta I=1$ which connect the unfavoured states to the favoured states with one aligned proton in the $h_{11/2}$ orbit. The signature dependence of the $B(E2; \Delta I=1)$ follows the rule expected from Eq. (2·52) when the vibrational contributions are neglected. For $^{157}$Ho and $^{159}$Tm where the chemical potentials are situated about the middle of the Nilsson states associated with the $h_{11/2}$ orbit, we have found that the vibrational effects are always such that the transitions from the favoured states are enhanced in comparison with those from the unfavoured states. This signature dependence of $B(E2; I \to I-1)$ is in agreement with the experimental data. The major origin of this signature dependent effect can be attributed to the mixing of the generalized-gamma vibrations with the signature $\alpha=1$ in the unfavoured states. The microscopic mechanism of this signature dependent effect will be discussed in detail in a separate paper.[29] The vibrational effects clearly seen in the 1qp band are much reduced in the 3qp band, because the collectivity of the generalized-gamma vibration becomes weaker in the 3qp band.

Experimental values[4] for the ratio $Q_t^{(1)}/Q_t^{(2)}$ in $^{157}$Ho are greater than one, and thus much larger than the calculated values shown in Fig. 9. The experimental signature dependence is also stronger, about a factor of two, than the calculated result. It is hard, however, to obtain such large values for this ratio in the theoretical calculation. In this connection, we note that our calculation well reproduces the magnitudes of the $E2$-transition moments with $\Delta I=2$ in the neighbouring nucleus $^{159}$Tm (see Fig. 10) for which both the stretched and unstretched $E2$-transition rates have been determined recently by life-time measurements.[7]

Calculated results for the ratio $Q_t^{(1)}/Q_t^{(2)}$ of the unstretched and stretched $E2$-transition moments in $^{165}$Lu are displayed and compared with the recent experimental data[8] in Fig. 11. It is seen that the calculation correctly reproduces the experimental magnitudes of this ratio. It is also seen that the signature dependence is weak in this nucleus with $N=94$.
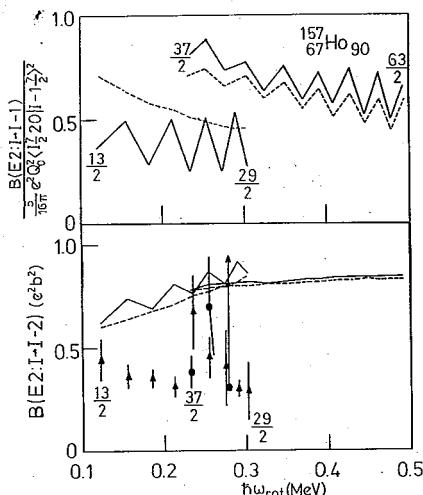
Fig. 9. $B(E2; I \rightarrow I-1)$ and $B(E2; I \rightarrow I-2)$ for
$^{157}$Ho, plotted as functions of $\omega_{rot}$. The solid
(broken) lines show the results of calculation in
which the coupling effects of the generalized-
gamma vibrations are taken into account
(neglected). The solid triangles and the solid
circles with error bars denote the experimental
data[4] for the 1qp and the 3qp band, re-
spectively. The $B(E2; I \rightarrow I-1)$ values are
shown in units of the rigid-rotor values $(5/16\pi)$
$\times \langle eQ_0 \rangle^2 \langle I, 7/2, 20|I-1, 7/2 \rangle^2$ in order to clear-
ly exhibit the signature dependence. The
experimental values for this quantity are lar-
ger than one and thus off scale.
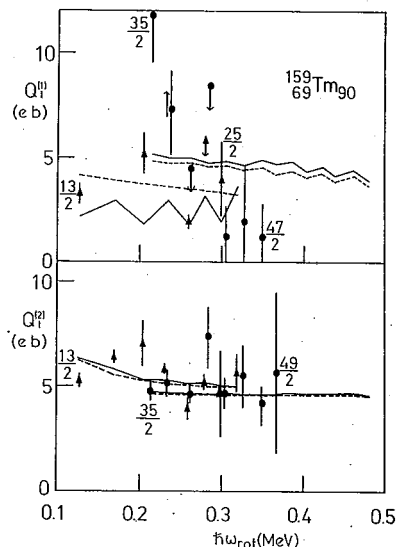
Fig. 10. $E2$-transition moments $Q_t^{(1)}$ and $Q_t^{(2)}$ for
$^{159}$Tm, plotted as functions of $\omega_{rot}$. They are
defined by

$$Q_t^{(\Delta I)} = \sqrt{\frac{(16\pi/5)B(E2; I \rightarrow I - \Delta I)}{\langle IK20|I - \Delta I, K \rangle^2}}.$$

The value $K = 7/2$ is used. Other notations are
the same as in Fig. 9. Experimental data are
taken from Ref. 7).

We note here that the calculated results presented above are consistent with those
of Ikeda[37] and Onishi et al.,[38] who previously pointed out the importance of the
contributions from the gamma-vibrations to the $M1$ and $E2$ transition matrix ele-
ments by treating them within the framework of the macroscopic Bohr-Mottelson-
type collective models.

In the calculation presented in Figs. 9~11, it is possible that the vibrational
effects are overestimated. The crucial quantities determining the magnitudes of
these effects are the quasiparticle-vibration-coupling vertices defined by Eq. (2·24).
It is known[39],[40] that the RPA calculation using the 5-major shells significantly
overestimates the $B(E2)$ values between the gamma-vibrational states and the ground
states in rare-earth nuclei. On the other hand, it seems reasonable to require that the
calculated coupling vertices should be independent of the truncation of the Nilsson
model space.[41] Then, it can be argued[42] that the 3-major shell calculation overes-
timates the magnitude of these vertices via the use of the force-strengths $\kappa_K^{(\pm)}$ (that
reproduce the experimental excitation energies of the $\beta$ and $\gamma$ vibrations within this
truncated model space) about 50% larger than those for the 5-major shell calculation,
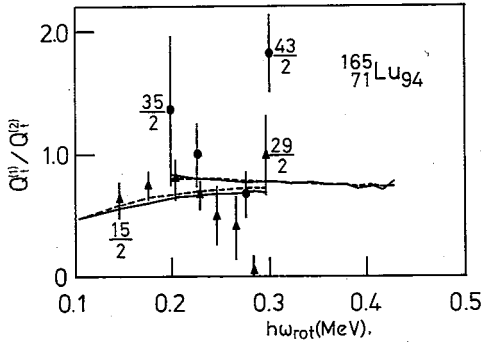even when the calculated $E2$ transition matrix elements $Q_K^{(\pm)}(n)$ correctly reproduce

Fig. 11.  Ratio $Q_t^{(1)}/Q_t^{(2)}$ of $E2$-transition moments for $^{165}$Lu, plotted as a function of $\omega_{rot}$. The value $K=9/2$ is used.  Other notations are the same as in Fig. 9.  Experimental data are taken from Ref. 8).

(within the 3-major shells) the experimental $B(E2)$ values between the gamma band and the $g$-band.

Experimental data for the $M1$ and $E2$ properties at a higher angular-momentum region are becoming available,[8] where various kinds of 5qp configurations may come into play.  In this region of angular momentum, the transition from the superconducting to the normal phases of the pairing correlation is expected to take place.  It remains to be an interesting subject to examine the applicability of 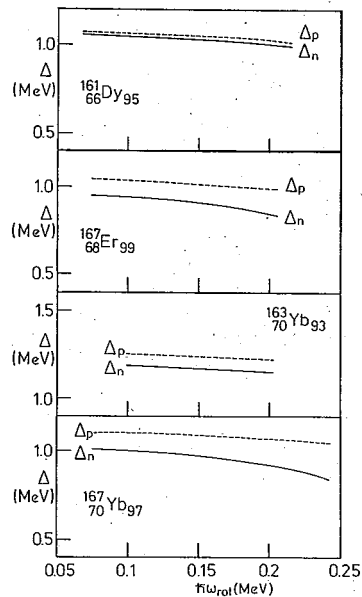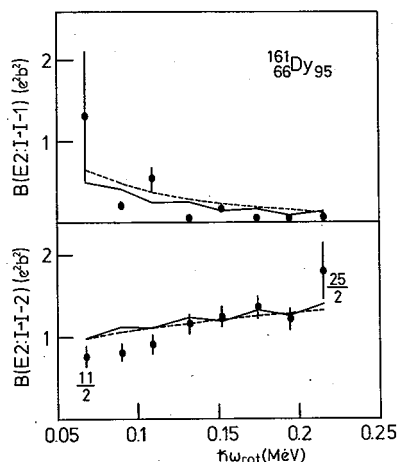the quasip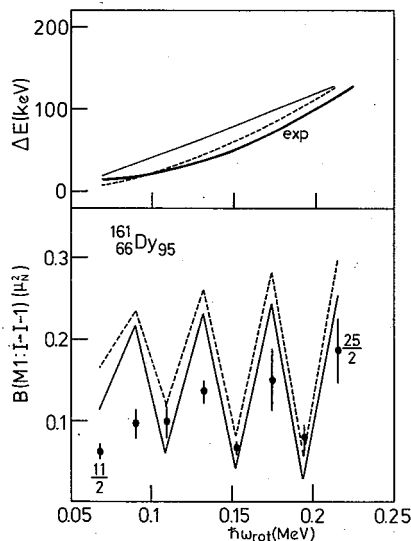article-vibration coupling model presented in this paper to such a transition region by taking into account the contributions from the pairing vibrational modes as well as the generalized-gamma vibrations.

### 4.3.  Nuclei with the $i_{13/2}$ odd neutron

The deformation parameters $(\beta_0, \gamma_0)$ calculated for the $g$-band configurations in $^{161}$Dy, $^{167}$Er and $^{161,163,167}$Yb are presented in Figs. 12 and 14.  These values are used in the quasiparticle-vibration-coupling calculations for the unique-parity bands associated with the $i_{13/2}$ odd neutron.  For these 1qp bands, the triaxiality parameter $\gamma_0$ is
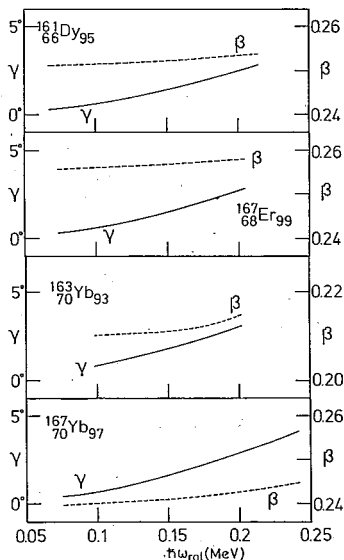


Fig. 12.  Deformation parameters $(\beta_0, \gamma_0)$ for the $g$-band configurations calculated as functions of $\omega_{rot}$. These values characterize the deformations of the "cores" of the odd-$N$ nuclei; $^{161}$Dy, $^{167}$Er and $^{163,167}$Yb.  Note that our definition of the sign of $\gamma_0$ is opposite to the Lund convention.[14]



Fig. 13.  Pairing gaps $(\Delta_p, \Delta_n)$ for the $g$-band configurations calculated as functions of $\omega_{rot}$. These values characterize the pairing deformations of the "cores" of the odd-$N$ nuclei; $^{161}$Dy, $^{167}$Er and $^{163,167}$Yb.
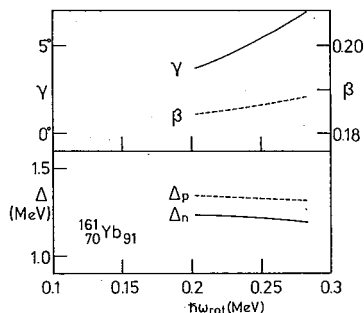
Fig. 14.  Same as Figs. 12 and 13 but for $^{161}$Yb.



Fig. 15.  $B(M1; I \to I-1)$ and the signature split-tings $\Delta E$ (absolute magnitudes) for $^{161}$Dy, plot-ted as functions of $\omega_{rot}$. Notations are the same as in Fig. 5. Experimental data are taken from Ref. 10). Theoretical $B(M1)$ values are those calculated by using $g_R = 0.21$. The sign of $\Delta E$ is negative, since the favoured signature $\alpha_f$ is $+1/2$ for the $i_{13/2}$ odd-quasiparticle in contrast to the $h_{11/2}$ odd-quasiparticle for which it is $-1/2$.



Fig. 16.  $B(E2; I \to I-1)$ and $B(E2; I \to I-2)$ for $^{161}$Dy, plotted as functions of $\omega_{rot}$. The solid circles with error bars denote the experimental data.[10] Other notations are the same as in Fig. 9.

positive (negative in the Lund convention) and gradually increases as a function of $\omega_{rot}$, but its magnitude remains small in the angular momentum region under consideration.

For the stable nuclei,$^{161}$Dy and $^{167}$Er, the $B(M1; I \to I-1)$, $B(E2; I \to I-1)$ and $B(E2; I \to I-2)$ values are separately known by Coulomb excitation experiments.[10],[11] Calculated results for these quantities are shown in Figs. 15~18 and compared with the experimental data.  Concerning the calculation of the $B(M1)$ values, we remark that the microscopically calculated values for the collective $g_R$-factor defined by Eq. (2·56) are $0.37 \sim 0.36$ for $^{161}$Dy and $0.32 \sim 0.28$ for $^{167}$Er in the rotational-frequency region under consideration.  However, for the magnitude of $B(M1)$, we find that much better agreement with the experimental data is obtainable if the phenomenologically determined values, 0.21 for $^{161}$Dy and 0.18 for $^{167}$Er, are used in place of the microscopically calculated $g_R$.  (The possible origins of decreasing the $g_R$ values in these nuclei are discussed in the textbook of Bohr and Mottelson.[3])  Thus, the $B(M1)$ values obtained by using the phenomenological $g_R$ are presented in Figs. 15 and 17.  It is seen that the signature dependence is well reproduced in the calculation.

Figures 16 and 18 clearly show that the magnitudes of the calculated $B(E2; I \to I-1)$ and $B(E2; I \to I-2)$ are in good agreement with the experimental data.  In
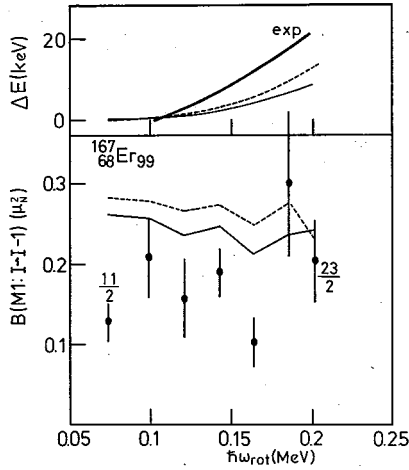
Fig. 17. Same as Fig. 15 but for $^{167}$Er. Experimental data are taken from Ref. 11). Theoretical $B(M1)$ values are those calculated by using $g_R = 0.18$.
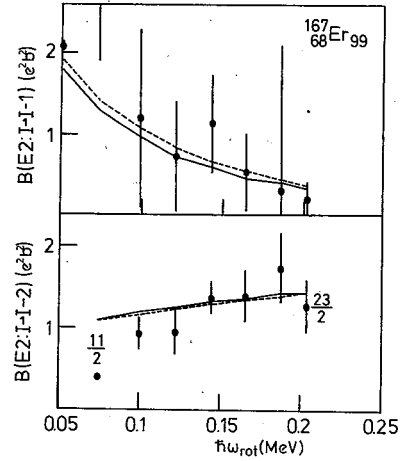


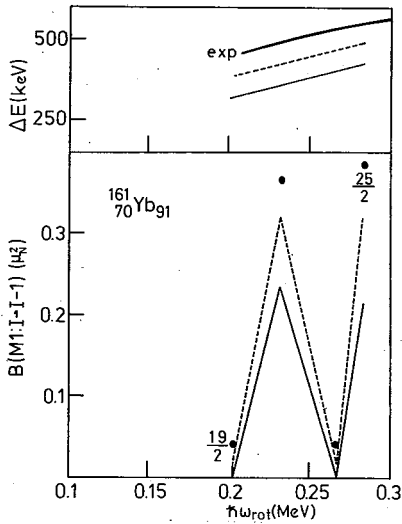Fig. 18. Same as Fig. 16 but for $^{167}$Er. Experimental data are taken from Ref. 11).



Fig. 19. Same as Fig. 15 but for $^{161}$Yb. Experimental $B(M1)$ values are those[12),13)] obtained by assuming appropriate values for $B(E2; I \to I-2)$. Theoretical $B(M1)$ values are those calculated by using $g_R = 0.2$.
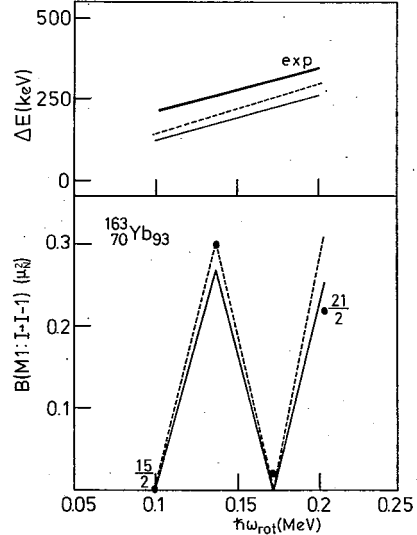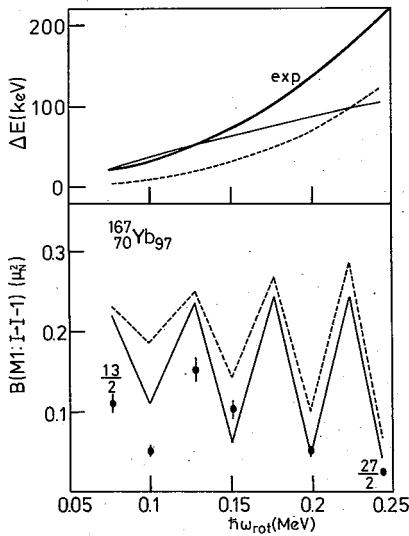


Fig. 20. Same as Fig. 19 but for $^{163}$Yb.

the calculation we find that the signature dependence of $B(E2; I \to I-1)$ is weak in the case of $^{161}$Dy and $^{167}$Er. This is because the static triaxiality $\gamma_0$ is small and also because the coupling effects from the generalized-gamma vibrations are weak in these nuclei. To test this result of calculation, we need more accurate data for $B(E2; I \to I-1)$ in $^{167}$Er. Of course, experimental data for the $M1$ and $E2$ properties of the 3qp bands in these odd-$N$ nuclei are very much desired.

Fig. 21. Same as Fig. 19 but for $^{167}$Yb.

Figures 19~21 show the calculated results for $B(M1; I \rightarrow I-1)$ in $^{161,163,167}$Yb. In these calculations, the phenomenological value $g_R = 0.2$ is used for the rotational $g$-factor. We see that the calculated signature splittings $\Delta E$ decrease as the neutron number increases from 91 to 97, in agreement with the experimental trend. The signature dependence of the $B(M1)$ values is also well reproduced in the calculation. The decrease of $\Delta E$ is a simple consequence of the increase of the deformation parameter $\beta$ with increasing $N$ (see Figs. 12 and 14).

## § 5. Concluding remarks

We have developed a microscopic model which takes into account both the static and dynamic triaxial deformations in the description of high-spin states of odd-$A$ nuclei. The model is based on the rotating shell model and treats the quasiparticle-vibration couplings in the uniformly rotating frame of reference. With the use of this model, we have discussed the effects of the static and dynamic triaxial deformations on the signature splitting of the quasiparticle energies and on the signature dependence of $B(M1)$, $B(E2; I \rightarrow I-1)$ and $B(E2; I \rightarrow I-2)$ values for the transitions within the unique-parity bands in the rare-earth odd-$A$ nuclei to which experimental data are available.

It has been shown that both the static and dynamic triaxial deformations bring about characteristic signature dependences in the $E2$-transition matrix elements. Thus, the $B(E2; I \rightarrow I-1)$ values are, in general, sensitive to whether these signature-dependent matrix elements add coherently or destructively. It has also been shown that the major effects of aligned quasiparticles on the $B(M1)$ values are easily taken into account through the change in the $g_{RPA}$ values. In particular, the increase of the $B(M1)$ values associated with the alignment of the $i_{13/2}$ neutrons in odd-$Z$ nuclei is qualitatively reproduced in the calculation. Thus, the microscopic model developed in this paper is useful to study the relation between the alignment and the triaxial deformations as well as their effects on the $M1$ and $E2$ transition properties at high-spin.

It is certainly a very interesting subject to further refine the microscopic model described in this paper; for instance, by taking into account higher-order quasiparticle-vibration-coupling diagrams. In view of the present status of experimental data, however, it seems for us more important to carry out a systematic comparison between theoretical calculations and experimental data within the framework of the model presented. More accurate and systematic data for the signature splittings, $B(M1)$, $B(E2; I \rightarrow I-1)$ and $B(E2; I \rightarrow I-2)$ are needed in order to identify

the static and dynamic triaxial deformations and to understand their roles in characterizing the high-spin spectra in the near-yrast region.

## Acknowledgements

### References

1)  L. S. Kisslinger and R. A. Sorensen, Rev. Mod. Phys. **35** (1963), 853.
2)  V. G. Soloviev, *Theory of Complex Nuclei* (Nauka, Moskow, 1971 [Transl. Pergamon Press, 1976]).
3)  A. Bohr and B. R. Mottelson, *Nuclear Structure*, vol. 2 (Benjamin, New York, 1975).
4)  G. B. Hagemann et al., Nucl. Phys. **A424** (1984), 365.
5)  A. J. Larabee et al., Phys. Rev. **C29** (1984), 1934.
6)  R. Holtzmann et al., Phys. Rev. **C31** (1985), 421.
7)  J. Gascon et al., Nucl. Phys. **A467** (1987), 539.
8)  G. B. Hagemann, private communication.
9)  P. Frandsen et al., Phys. Lett. **B177** (1986), 287.
10)  M. Oshima et al., to be published.
11)  M. Ohshima et al., Nucl. Phys. **A436** (1985), 518.
12)  N. Roy et al., Nucl. Phys. **A382** (1982), 125.
13)  J. Kownacki et al., Nucl. Phys. **A394** (1983), 269.
14)  I. Hamamoto, *Proc. Niels Bohr Centennial Conf. on Nuclear Structure, Copenhagen 1985*, ed. R. Broglia, G. B. Hagemann and B. Herskind (North-Holland, 1985), p. 129, and references therein.
15)  I. Hamamoto and B. Mottelson, Phys. Lett. **132B** (1983), 7.
16)  Y. R. Shimizu and K. Matsuyanagi, Prog. Theor. Phys. **70** (1983), 144.
17)  Y. R. Shimizu and K. Matsuyanagi, Prog. Theor. Phys. **72** (1984), 799.
18)  R. Bengtsson and S. Frauendorf, Nucl. Phys. **A327** (1979), 139.
19)  S. Frauendorf, in *Nuclear Physics*, ed. C. H. Dasso, R. A. Broglia and A. Winther (North-Holland, 1982), p. 111.
20)  E. R. Marshalek, Nucl. Phys. **A275** (1977), 416.
21)  T. Marumori, T. Maskawa, F. Sakata and A. Kuriyama, Prog. Theor. Phys. **64** (1980), 1294.
22)  Y. R. Shimizu, to be published.
23)  Y. R. Shimizu and K. Matsuyanagi, Prog. Theor. Phys. **74** (1985), 1346, and to be published.
24)  J. D. Garrett, G. B. Hagemann and B. Herskind, Annu. Rev. Nucl. and Part. Sci. **36** (1986), 419.
25)  Y. R. Shimizu and K. Matsuyanagi, Prog. Theor. Phys. **71** (1984), 960.
26)  E. R. Marshalek, Phys. Rev. **C11** (1975), 1426.
27)  E. R. Marshalek, Nucl. Phys. **A331** (1979), 429.
28)  K. Hara and S. Kusuno, Nucl. Phys. **A245** (1975), 147.
29)  M. Matsuzaki, Y. R. Shimizu and K. Matsuyanagi, in preparation.
30)  D. Janssen and I. N. Mikhailov, Nucl. Phys. **A318** (1979), 390.
31)  S. Frauendorf, Phys. Lett. **100B** (1981), 219.
32)  I. Hamamoto and B. Mottelson, Phys. Lett. **167B** (1986), 370.
33)  Y. S. Chen, P. B. Semmes and G. A. Leander, Phys. Rev. **C34** (1986), 1935.
34)  J. Billowes et al., Phys. Lett. **178B** (1986), 145.
35)  S. Frauendorf and F. R. May, Phys. Lett. **125B** (1983), 245.
36)  M. Matsuzaki, Y. R. Shimizu and K. Matsuyanagi, Prog. Theor. Phys. **77** (1987), 1302.
37)  A. Ikeda, Nucl. Phys. **A439** (1985), 317.
38)  N. Onishi, I. Hamamoto, S. Åberg and A. Ikeda, Nucl. Phys. **A452** (1986), 71.
39)  T. S. Dumitrescu and I. Hamamoto, Nucl. Phys. **A383** (1982), 205.

40)   Y. R. Shimizu and K. Matsuyanagi, Prog. Theor. Phys. **72** (1984), 1017.
41)   M. Matsuo and K. Matsuyanagi, Prog. Theor. Phys. **78** (1987), 591.
42)   I. Hamamoto, private communication.

**Note added in proof :**

1)   The operators $\hat{D}^{\lambda}_{\mu\nu}$ used in Eq. (2·35) are equivalent to the $\hat{D}^{\lambda}_{\nu\mu}$ operators of Ref. 20).

2)   The quadrupole matrix elements, $Q^{(-)}_{k}(\mu\bar{\nu})$ and $Q^{(-)}_{k}(n)$, appearing in Eqs. (2·43) and (2·44) should be distinguished from the doubly stretched ones appearing in Eqs. (2·24)~(2·30), although the same notations are used for these different quantities.

3)   In the actual numerical calculation, the angular momentum $I_0$ defined by Eq. (2·33) is used in place of the $I_c \equiv \langle \hat{J}_x \rangle$ appearing in the expressions for the intrinsic $E2$ operator $Q^{(\mathrm{PA})}_{2x}$. This replacement may be allowed for the Ho, Tm and Lu nuclei, in which the difference $(I_0-I_c)$ arising from the aligned angular momentum of the $h_{11/2}$ proton is rather small $(1 \sim 2\hbar)$. When this difference cannot be neglected, more careful treatment of these quantities will be required.